Composite synoptic-scale environments conducive to North American polar/subtropical jet superposition events

By

ANDREW C. WINTERS[1*], DANIEL KEYSER[2], LANCE F. BOSART[2], and JONATHAN E. MARTIN[3]

[1]Department of Atmospheric and Oceanic Sciences
University of Colorado Boulder
Boulder, CO 80309

[2]Department of Atmospheric and Environmental Sciences
University at Albany, State University of New York
Albany, NY 12222

[3]Department of Atmospheric and Oceanic Sciences
University of Wisconsin – Madison
Madison, WI 53706

Submitted for publication in *Monthly Weather Review*
XX August 2019

[*] *Corresponding author address:* Andrew C. Winters, Dept. of Atmospheric and Oceanic Sciences, University of Colorado Boulder, Street Address., Boulder, CO 80309. E-mail: acwinters@albany.edu

ABSTRACT

While the Northern Hemisphere polar and subtropical jet streams typically reside in different climatological latitude bands, the separation between the two jets occasionally vanishes resulting in a polar/subtropical jet superposition. The development of a jet superposition represents the creation of a dynamical and thermodynamic environment that is particularly conducive to the production of high-impact weather. The synoptic-scale environments that support the development of North American jet superpositions can vary considerably, however, depending on the case under consideration. This observation motivates a comprehensive examination of the varied synoptic-dynamic mechanisms that operate within a double-jet environment to produce North American jet superpositions. This study objectively identifies North American jet superposition events during November–March 1979–2010 and subsequently classifies those events into three characteristic event types. "Polar dominant" events are those during which only the polar jet is characterized by a substantial excursion from its climatological latitude band, "subtropical dominant" events are those during which only the subtropical jet is characterized by a substantial excursion from its climatological latitude band, and "hybrid" events are those characterized by a mutual excursion of both jets from their respective climatological latitude bands. Composite analyses performed on each event type reveal the important role that descent plays in restructuring the tropopause beneath the confluent jet-entrance region prior to each jet superposition event type. Additionally, surface cyclogenesis and implied diabatic heating tend to lead and directly contribute to the development of subtropical dominant superpositions, while those processes tend to maximize concurrently with and downstream of polar dominant superpositions.

1. Introduction

The instantaneous positions of the polar and subtropical jets are closely related to the pole-to-equator tropopause structure (e.g., Defant and Taba 1957; Palmén and Newton 1969; Shapiro et al. 1987). In the Northern Hemisphere, the polar jet is located near 50°N in the region where the tropopause height abruptly rises from the polar tropopause (~350 hPa) to the subtropical tropopause (~250 hPa). The polar jet sits atop the strongly baroclinic, tropospheric-deep polar front (e.g., Palmén and Newton 1948; Namias and Clapp 1949; Newton 1954; Palmén and Newton 1969, Keyser and Shapiro 1986; Shapiro and Keyser 1990) and arises due to the eddy momentum flux convergence that accompanies developing baroclinic waves (e.g., Held 1975; Rhines 1975; McWilliams and Chow 1981; Panetta 1993). The subtropical jet is located equatorward of the polar jet near 30°N in the region where the tropopause height abruptly rises from the subtropical tropopause to the tropical tropopause (~100 hPa). The subtropical jet features modest baroclinicity in the upper troposphere and lower stratosphere, and arises due to the poleward transport of angular momentum by the Hadley circulation (e.g., Loewe and Radok 1950; Yeh 1950; Koteswaram 1953; Mohri 1953; Koteswaram and Parthasarathy 1954; Sutcliffe and Bannon 1954; Krishnamurti 1961; Riehl 1962; Held and Hou 1980).

While the polar and subtropical jets typically occupy separate climatological latitude bands, the latitudinal separation between the two jet streams occasionally vanishes resulting in a polar/subtropical jet superposition (e.g., Winters and Martin 2014, 2016, 2017; Handlos and Martin 2016; Christenson et al. 2017). A cross section perpendicular to the axis of an observed jet superposition at 1200 UTC 20 December 2009 highlights the leading characteristics of a jet superposition (Figs. 1a,b). These characteristics include the development of (1) a steep, two-step pole-to-equator tropopause structure, (2) anomalously strong wind speeds that can exceed 100 m

s^{-1} in some instances, and (3) strong baroclinicity in the upper troposphere and lower stratosphere as required by thermal wind balance. The development of strong baroclinicity attendant to the jet superposition is also accompanied by the formation of a vigorous across-front ageostrophic circulation that can directly influence the production of high-impact weather (e.g., Winters and Martin 2014, 2016, 2017).

Christenson et al. (2017) objectively identified jet superpositions during the cold season (November–March) within the 2.5°-resolution NCEP–NCAR Reanalysis dataset (Kalnay et al. 1996; Kistler et al. 2001), and examined the climatological frequency of Northern Hemisphere jet superpositions during 1960–2010. Their analysis indicates that jet superpositions are most frequent in three locations: the western North Pacific, North America, and Northern Africa. Handlos and Martin (2016) provide a detailed examination of the key dynamical processes associated with western North Pacific jet superpositions. These key dynamical processes include equatorward surges of lower-tropospheric cold air over the east Asian continent that strengthen the lower-tropospheric baroclinicity at middle and subtropical latitudes, and the development of widespread convection over the western equatorial Pacific.

Prior work concerning North American jet superpositions, however, has focused solely on individual case studies. Winters and Martin (2014, 2016) examined the development of a jet superposition during the 1–3 May 2010 Tennessee Flood, and determined that a substantial fraction of the poleward moisture transport into the southeastern U.S. prior to the second day of the event was accomplished via the across-front ageostrophic circulation associated with the superposed jet. This poleward moisture transport ensured that heavy precipitation continued unabated during the second day of the event. The presence of widespread convection during the 2010 Tennessee Flood also contributed to the diabatic erosion of upper-tropospheric potential

114 vorticity (PV) on the equatorward side of the subtropical jet, which facilitated a poleward shift in
115 the position of the subtropical waveguide and the formation of the steep, two-step tropopause
116 structure that accompanied the superposition.

117 Winters and Martin (2016, 2017) performed a complementary analysis of a wintertime jet
118 superposition event at 1200 UTC 20 December 2009 (Fig. 1) that featured a rapidly-deepening
119 surface cyclone beneath the poleward-exit region of the superposed jet. This cyclone was
120 associated with snowfall totals in excess of 30 cm (~1 ft) in locations ranging from the Mid-
121 Atlantic northeastward towards New England. In contrast to the 2010 Tennessee Flood,
122 widespread convection on the equatorward side of the subtropical jet did not play a substantial
123 role in facilitating the development of the superposed jet's two-step tropopause structure in this
124 case. Instead, Winters and Martin (2016, 2017) determined that the descending branch of an
125 across-front ageostrophic circulation within the double-jet environment played the dominant role
126 in restructuring the tropopause prior to superposition.

127 These two cases served as the foundation for the conceptual model of North American jet
128 superpositions (Fig. 2) introduced by Winters and Martin (2017; their Fig. 2). In this model, jet
129 superposition features the development of a polar cyclonic PV anomaly at high latitudes with a
130 polar jet streak located equatorward of the PV anomaly. Polar cyclonic PV anomalies, which
131 include coherent tropopause disturbances (e.g., Hakim 2000; Pyle et al. 2004) and tropopause
132 polar vortices (e.g., Cavallo and Hakim 2009, 2010, 2012, 2013), typify a dynamical
133 environment that can be particularly conducive to surface cyclogenesis at middle and high
134 latitudes (i.e., Hakim et al. 1995, 1996; Pyle et al. 2004; Cavallo and Hakim 2010).

135 Jet superposition also features the concomitant production of a tropical anticyclonic PV
136 anomaly on the equatorward side of the subtropical jet. Tropical anticyclonic PV anomalies

result from the poleward transport of tropical, low-PV upper-tropospheric air via tropical plumes, low-latitude troughs, and/or tropical cyclones (e.g., Iskenderian 1995; Roundy et al. 2010; Fröhlich et al. 2013; Archambault et al. 2013, 2015; Winters and Martin 2016). The presence of tropical anticyclonic PV anomalies at midlatitudes typifies a thermodynamic environment characterized by weak upper-tropospheric static stability, and an environment that may feature an atmospheric river (e.g., Newell et al. 1992; Zhu and Newell 1998; Ralph et al. 2004, 2018, 2019) within the poleward-directed branch of the anticyclonic PV anomaly's tropospheric-deep circulation.

If polar cyclonic and tropical anticyclonic PV anomalies are situated within a confluent large-scale flow pattern and phase favorably, the result is a meridional juxtaposition of the two PV anomalies at midlatitudes. This configuration encourages constructive interference between the nondivergent circulations that accompany each PV anomaly and the rapid acceleration of wind speeds in the area between the two anomalies. The meridional juxtaposition of these two PV anomalies also represents the creation of a dynamical and thermodynamic environment that is particularly conducive to high-impact weather. Once the two PV anomalies are meridionally juxtaposed, mesoscale processes within the near-jet environment, such as across-front ageostrophic circulations (e.g., Shapiro 1981, 1982; Keyser and Pecnick 1985; Keyser and Shapiro 1986; Rotunno et al. 1994; Schultz and Doswell 1999; Schultz and Sanders 2002; Lang and Martin 2012; Martin 2014; Handlos and Martin 2016; Winters and Martin, 2016, 2017) and the diabatic heating that accompanies widespread precipitation (e.g., McTaggart-Cowan 2001, 2004, 2007; Lee and Kim 2003; Agustí-Panareda et al. 2004; Ahmadi-Givi et al. 2004; Son and Lee 2005; Grams et al. 2011, 2013; Archambault et al. 2013, 2015; Lang and Martin 2013; Grams and Archambault 2016; Handlos and Martin 2016; Winters and Martin 2016, 2017), can

160 act to restructure the tropopause locally to produce the steep, two-step tropopause structure
161 associated with a superposition.
162 While this conceptual model generalizes the process of jet superposition over North
163 America, it does not acknowledge the variable roles that mesoscale processes can play during the
164 production of individual jet superposition events (e.g., Winters and Martin 2016; 2017).
165 Furthermore, the conceptual model in Fig. 2 conceals variability concerning the spectrum of
166 interactions that can occur between polar cyclonic and tropical anticyclonic PV anomalies prior
167 to jet superposition. For instance, an individual jet superposition can arise solely due to a
168 substantial equatorward deviation of the polar jet towards the latitude of the subtropical jet, and
169 vice versa. Therefore, this study adopts a comprehensive approach to examine the multiple
170 "flavors" of North American jet superpositions in greater detail, with the goal of determining the
171 variety of dynamical processes and large-scale evolutions that result in North American jet
172 superpositions.
173 The remainder of this manuscript is structured as follows. Section 2 discusses the
174 objective identification scheme used to identify jet superposition events, as well as the
175 classification scheme employed to partition jet superposition events into characteristic event
176 types. Section 3 discusses the climatological characteristics of each jet superposition event type.
177 Section 4 discusses the composite large-scale flow evolutions associated with the jet
178 superposition event types, and section 5 offers a summary of the most salient results from this
179 study.
180

181 **2. Data and Methodology**

182 This study employs data from the 0.5°-resolution National Centers for Environmental

183 Prediction Climate Forecast System Reanalysis (CFSR; Saha et al. 2010) at 6-h intervals during
184 the period, 1979–2010. This temporal period is chosen to ensure that our analysis period overlaps
185 entirely with the period examined in Christenson et al. (2017), while the CFSR is chosen to
186 obtain a finer resolution of the dynamical evolutions that precede jet superpositions compared to
187 the 2.5°-resolution NCEP–NCAR reanalysis used in prior examinations of superpositions (e.g.,
188 Handlos and Martin 2016; Christenson et al. 2017). All CFSR data were bilinearly interpolated
189 onto isentropic surfaces between 300 K and 380 K at 5-K intervals to accommodate the
190 forthcoming jet superposition identification scheme. This study also utilizes the 2.5°-resolution
191 NOAA Interpolated Outgoing Longwave Radiation (OLR) dataset (Liebmann and Smith 1996)
192 to construct daily composites of OLR for each jet superposition event type. Areas characterized
193 by negative OLR anomalies serve as proxies for the location of extensive cloud cover and may
194 imply the presence of precipitation at midlatitudes if the anomalies overlap with a favorable
195 dynamic and thermodynamic environment for large-scale ascent.

196 *a) Jet Superposition Event Identification*

197 The objective jet superposition identification scheme used in this study is identical to that
198 described in Winters and Martin (2014, 2016), Handlos and Martin (2016), and Christenson et al.
199 (2017). While the forthcoming discussion provides a brief conceptual overview of the
200 identification scheme, the reader is referred to the aforementioned studies for additional detail.

201 The identification of jet superpositions within the CFSR is grid-column based, in that the
202 scheme identifies grid columns that exhibit characteristics of both a polar and a subtropical jet. A
203 polar (subtropical) jet is identified within a grid column if two criteria are satisfied. First, the
204 integrated wind speed within that grid column must exceed 30 m s^{-1} within the 100–400-hPa
205 layer. Second, the magnitude of the horizontal PV gradient within the 1–3-PVU channel at that

grid column must exceed an empirically-defined threshold[1] in the 315–330-K (340–355-K) isentropic layer. A strong horizontal PV gradient in the 315–330-K (340–355-K) isentropic layer corresponds to the presence of a "break" between the polar and subtropical tropopauses (subtropical and tropical tropopauses). The identification of a polar and a subtropical jet within the same grid column of CFSR data at a single analysis time results in the identification of a jet superposition within that grid column, and is interpreted physically as the formation of a steep, two-step tropopause structure (e.g., Fig. 1b). On a horizontal map, this scheme is manifest at a single analysis time as a ribbon of positively-identified grid columns that parallel the axis of a superposed jet (not shown).

North American jet superpositions were isolated during the cold season (November–March) for this study within a domain bounded in latitude from 10° to 80°N and in longitude from 140°W to 50°W. While jet superpositions do occur outside of the cold season (e.g., the 2010 Tennessee Flood), the aforementioned identification scheme would require modifications to account for the vertical movement of the polar and subtropical jet cores throughout the year in order to comprehensively identify jet superpositions during the fall and spring. An effort to investigate the general character of North American jet superpositions during the fall and spring is outside the scope of the present study and is reserved for future work.

Following their identification, all 6-h analysis times characterized by a superposition were filtered to retain only those times that rank in the top 10% in terms of the number of grid columns characterized by a jet superposition (≥18 grid columns). This filter retains only those situations in which the polar and subtropical jets are superposed for a substantial distance along the jet axis. All grid columns characterized by a jet superposition during a retained analysis time

[1] The specific threshold used for the magnitude of the horizontal PV gradient within the 315–330-K (340–355-K) isentropic layer is 1.4×10^{-5} PVU m^{-1} (0.9×10^{-5} PVU m^{-1}), where 1 PVU = 10^{-6} K m^2 kg^{-1} s^{-1}.

were also required to be located within 1000 km of another grid column characterized by a superposition. If an analysis time featured a group of 18 or more grid columns that satisfied this distance criterion, it was labeled a "jet superposition event". Note that this methodology allows for the identification of multiple jet superposition events at a single analysis time, so long as the groups of jet superposition grid columns are more than 1000 km apart and each group is ≥ 18 grid columns in size.

The latitude and longitude of each grid column associated with a jet superposition event were averaged to compute a latitude-longitude centroid for that particular event. The positions of the event centroids were then compared across all events to group together jet superposition events that may be associated with the same jet structure. In particular, if an event centroid during one event was located within 1500 km of another event centroid during the previous 30-h period, those jet superposition events were considered to be the same event. The methodology described above produced a total of 326 jet superposition events.

b) Jet Superposition Event Classification

Following their identification, jet superposition events were classified into event types based on the degree to which the polar and subtropical jets deviated from their respective climatological positions to form a superposition. The climatological position of the polar (subtropical) waveguide at a single analysis time (e.g., 0000 UTC 1 January) was calculated by averaging the position of the 2-PVU contour on the 320-K (350-K) isentropic surface at 24-h intervals within a 21-day window centered on that analysis time for every year between 1979 and 2010. The 320- and 350-K isentropes reside firmly within the isentropic layers used to identify the polar and subtropical jets, respectively, and serve as reasonable proxies for the positions of

250 the polar and subtropical waveguides during the cold season (e.g., Martius et al. 2010;
251 Christenson et al. 2017).
252 The event classification scheme subsequently compares the position of each jet
253 superposition event centroid against the climatological positions of both the polar and subtropical
254 waveguides at the start of an event. "Polar dominant" events (Fig. 3a) are those events in which
255 an observation of 2 PVU at the location of the event centroid represents a standardized PV
256 anomaly > 0.5 on the 320-K isentropic surface and a standardized PV anomaly > –0.5 on the
257 350-K isentropic surface. Consequently, polar dominant events exhibit a substantial equatorward
258 deviation of the polar jet from its climatological position to superpose with the subtropical jet
259 near its climatological position. "Subtropical dominant" events (Fig. 3c) are those events in
260 which an observation of 2 PVU at the location of the event centroid represents a standardized PV
261 anomaly < 0.5 on the 320-K isentropic surface and a standardized PV anomaly < –0.5 on the
262 350-K isentropic surface. Subtropical dominant events exhibit a substantial poleward deviation
263 of the subtropical jet from its climatological position to superpose with the polar jet near its
264 climatological position. "Hybrid" events (Fig. 3b) are those events in which an observation of 2
265 PVU at the location of the event centroid represents a standardized PV anomaly > 0.5 on the
266 320-K isentropic surface and a standardized PV anomaly < –0.5 on the 350-K isentropic surface.
267 Hybrid events, therefore, exhibit a mutual deviation of the polar and subtropical jets from their
268 respective climatological positions to form a superposition. These categories of jet superposition
269 events represent the spectrum of interactions that can occur between PV anomalies along the
270 polar and subtropical waveguides prior to jet superpositions, and the climatological
271 characteristics of events within these categories will be the focus for the remainder of the study.
272

3. Jet Superposition Event Type Characteristics

The monthly frequency of North American jet superposition events as a function of event type are shown in Fig. 4. Overall, jet superposition events are most frequent during the months of November and December, and taper off during the remaining months of the cold season. This result is consistent with the findings of Christenson et al. (2017; their Fig. 6), whose analysis shows a broader spatial coverage of North American jet superpositions during November and December compared to January, February, and March. Figure 4 also indicates that subtropical dominant events (N=129) are favored by roughly a 3:2 margin compared to polar dominant events (N=80), suggesting that substantial poleward excursions of the subtropical jet to superpose with the polar jet are more common than the converse evolution. The largest disparity between polar dominant and subtropical dominant events occurs during November and December, when subtropical dominant events are clearly the most frequent event type. Hybrid events (N=117), however, are the most frequent event type during January, February, and March.

Figure 5 illustrates the spatial frequency of jet superposition events as a function of event type. Polar dominant events (Fig. 5a) are most frequent along the U.S./Mexico border and along the northern coast of the Gulf of Mexico. The branch of higher frequencies extending towards the northeast U.S. is representative of those polar dominant events that initially develop at low latitudes and propagate downstream within upper-tropospheric southwesterly flow. This evolution is further apparent considering the statistics provided in Table 1. Namely, the average polar dominant event develops at subtropical latitudes (e.g., 29.7°N; 102.0°W). The third and fourth columns of Table 1 reveal the average translation of an individual jet superposition event centroid in latitude-longitude space during its lifespan. A consideration of polar dominant events indicates a northeastward translation in the position of those events throughout their lifespan,

296 consistent with the branch of higher frequencies that extend towards the northeast U.S in Fig. 5a.
297 Hybrid events (Fig. 5b) are most frequent within a 5°-latitude band ranging from 35°N to 40°N,
298 with the largest number of events situated over the southeastern U.S. and western North Atlantic.
299 Hybrid events (34.5°N; 94.3°W) initially develop farther northeast of polar dominant events and
300 translate in a more zonal direction compared to polar dominant events (Table 1).
301 Subtropical dominant events (Fig. 5c) are characterized by two separate frequency
302 maxima centered on the eastern and western coasts of North America, respectively.
303 Consequently, the average location of jet superposition for subtropical dominant events (46.7°N;
304 92.1°W) is not representative of the frequency distribution shown in Fig. 5c. This observation
305 motivated partitioning subtropical dominant events into an "eastern" and "western" category
306 based on the position of each individual event centroid relative to the 96°W meridian at the start
307 of an event. A comparison of the relative frequencies of eastern and western subtropical
308 dominant events shows that eastern events (N=76) are more common than western events
309 (N=53). Furthermore, eastern (48.5°N; 71.2°W) and western (44.0°N; 122.1°W) subtropical
310 dominant events develop at higher latitudes compared to polar dominant and hybrid events, and
311 both subtropical dominant event types translate in a southeastward direction following their
312 development. The latter result suggests that subtropical dominant events often develop at the
313 apex of upper-tropospheric ridges and subsequently propagate downstream within upper-
314 tropospheric northwesterly flow.
315
316 **4. Jet Superposition Event Type Composites**
317 Composite analyses were constructed for each jet superposition event type to examine the
318 synoptic-scale flow evolution during the 48-h period prior to jet superposition. All composites

were calculated by shifting the CFSR and OLR data for each event so that each individual event centroid was collocated with the average starting latitude and longitude for its corresponding event type (Table 1). All CFSR and OLR data were weighted by the cosine of latitude before they were shifted, and a weighted average of the shifted CFSR and OLR data was calculated at each grid point within a domain bounded in latitude from 10°N to 80°N and in longitude from 150°E to 10°W to construct the event composites. A two-sided Student's *t*-test was performed on the composite 250-hPa geopotential height, precipitable water, and mean sea level pressure anomalies to identify regions that are statistically distinct from climatology at the 99% confidence level (Wilks 2011). The primary focus of the forthcoming discussion is to determine the dynamical processes that facilitate the development of a steep, two-step tropopause structure during polar, eastern subtropical, and western subtropical dominant superpositions. Hybrid events are not considered further, as the dynamical processes facilitating superposition during those events can be conceptualized as a combination of the processes diagnosed during polar, eastern subtropical, and western subtropical dominant events.

a) Polar Dominant Events

48 h prior to superposition, a surface cyclone is situated in a favorable region for synoptic-scale ascent beneath the poleward-exit region of a zonally-extended and poleward-shifted North Pacific jet stream (Figs. 6a,b). Perturbation upper-tropospheric ridges are located farther downstream over the eastern North Pacific and eastern Canada, respectively, and a perturbation upper-tropospheric trough is positioned over the southwestern U.S. at this time. A weak surface cyclone is in a favorable location for further development downstream of the southwestern U.S. trough and is associated with a zonally-oriented band of negative OLR anomalies. These OLR anomalies are suggestive of increased cloud cover along the developing

342 warm-frontal boundary attendant to the surface cyclone (not shown).

343 The eastern North Pacific ridge amplifies 24 h prior to superposition in conjunction with
344 lower-tropospheric warm-air advection and implied diabatic heating within the warm sector of
345 the surface cyclone in the Gulf of Alaska (Figs. 6c,d). The axis of the eastern North Pacific ridge
346 exhibits a positive tilt at this time, indicating a preference for anticyclonic wave breaking to
347 precede polar dominant superpositions. Anticyclonic wave breaking over the eastern North
348 Pacific subsequently contributes to further amplification of the southwestern U.S. trough 24 h
349 prior to superposition.

350 A maximum in 300-hPa geostrophic warm-air advection is situated downstream of the
351 southwestern U.S. trough 24 h prior to superposition (Fig. 6c), implying that the thermally-
352 indirect circulation within the exit region of the developing superposed jet is shifted equatorward
353 so as to position ascent beneath the jet core (e.g., Shapiro 1981, 1982; Lang and Martin 2012,
354 2013). In response to a favorable environment for synoptic-scale ascent provided by the
355 thermally-indirect circulation within the jet-exit region and the proximity of the southwestern
356 U.S. trough (Figs. 6a,c), the surface cyclone intensifies during the intervening 24-h period (Figs.
357 6b,d). Perturbation southerly geostrophic flow that accompanies the intensified surface cyclone
358 subsequently results in the development of a corridor of anomalous precipitable water within the
359 cyclone's warm sector (Fig. 6d). The collocation of precipitable water anomalies, negative OLR
360 anomalies, and implied ascent within the surface cyclone's warm sector suggests that widespread
361 precipitation accompanies the surface cyclone at this time. Consequently, implied diabatic
362 heating in the vicinity of the surface cyclone likely contributes to an amplification of the
363 downstream ridge over eastern North America by the time of superposition (Fig. 6e).

364 Strengthened 300-hPa geostrophic warm-air advection and enhanced flow curvature

365 downstream of the deep upper-tropospheric trough over the southern Plains at the time of
366 superposition imply that synoptic-scale ascent continues unabated in the vicinity of the surface
367 cyclone during the 24-h period prior to superposition (Figs. 6c,e). As a result, the surface cyclone
368 reaches maximum intensity at the time of superposition (Fig. 6f). Precipitable water anomalies
369 and negative OLR anomalies in the vicinity of the surface cyclone also achieve their maximum
370 magnitudes at this time, suggesting that precipitation maximizes in both intensity and areal
371 coverage concurrently with the formation of a superposition. Any implied areas of precipitation
372 associated with the surface cyclone are located exclusively downstream of the jet superposition
373 event centroid, however (Fig. 6f). Consequently, diabatic heating is likely located too far
374 downstream to play a direct role in the formation of the two-step tropopause structure that
375 accompanies polar dominant jet superpositions. Diabatic heating likely plays an *indirect* role in
376 facilitating superposition via its contribution to the amplification of the upper-tropospheric ridge
377 over eastern North America. Namely, downstream flow amplification slows the eastward
378 translation speed of the upper-tropospheric trough over the southern Plains, allowing additional
379 time for the superposition to develop at the base of the trough.

380 Upstream of the jet superposition centroid, the upper-tropospheric flow pattern is
381 characterized by 300-hPa geostrophic cold-air advection that initially develops 24 h prior to
382 superposition (Figs. 6c,e). The presence of geostrophic cold-air advection suggests that the
383 thermally-direct circulation within the jet-entrance region is shifted equatorward so as to position
384 descent beneath the jet core. Labeled the "Shapiro effect" by Rotunno et al. (1994), descent
385 beneath the jet core is strongly conducive to upper-tropospheric frontogenesis and the
386 concomitant development of a tropopause fold (i.e., Shapiro 1981, 1982; Keyser and Pecnick
387 1985; Keyser and Shapiro 1986; Rotunno et al. 1994; Schultz and Doswell 1999; Schultz and

Sanders 2002; Lang and Martin 2012; Martin 2014; Winters and Martin 2016, 2017). Consequently, descent beneath the jet-entrance region appears to play a direct role in the formation of the steep, two-step tropopause structure associated with a polar dominant jet superposition.

To investigate this assertion more rigorously, a series of vertical cross sections were constructed upstream of the developing superposed jet and perpendicular to the jet axis 12 h prior to superposition (B–B') and at the time of superposition (C–C'). Consistent with the presence of 300-hPa geostrophic cold-air advection, these cross sections highlight a region of focused descent beneath and poleward of the jet core 12 h prior to superposition (Fig. 7a) and at the time of jet superposition (Fig. 7b). This descent accounts for a large fraction of the positive PV advection diagnosed along the dynamic tropopause at both times and, consequently, for a downward penetration of high-PV air from the lower stratosphere during the 12-h period prior to superposition (Figs. 7a,b). The downward penetration of high-PV air completes the production of the steep, two-step tropopause structure (Fig. 7b) that must accompany the superposition.

The cross sections also highlight the presence of a strong cyclonic PV anomaly on the poleward side of the jet that intensifies in magnitude during the 12-h period prior to superposition (Figs. 7a,b). Notably, the cross sections only highlight a weak anticyclonic PV anomaly above 200 hPa on the equatorward side of the jet. Consequently, the anomalously strong wind speeds that accompany a polar dominant jet superposition are driven disproportionately by the nondivergent circulation that accompanies the strong polar cyclonic PV anomaly. The lack of a strong anticyclonic PV anomaly on the equatorward side of the jet is not surprising, given that this event type requires a superposition to develop at the climatological latitude of the subtropical jet. This result, however, indicates that knowledge of the creation and

411 subsequent transport of polar cyclonic PV anomalies towards subtropical latitudes is essential
412 towards diagnosing the development of a polar dominant jet superposition.

413 *b) Eastern Subtropical Dominant Events*

414 The composite large-scale flow pattern 48 h prior to an eastern subtropical dominant
415 event features a zonally oriented upper-tropospheric trough-ridge couplet centered over eastern
416 North America (Fig. 8a). A surface cyclone is favorably positioned within a region of synoptic-
417 scale ascent immediately downstream of the upper-tropospheric trough and beneath the jet-
418 entrance region, with a surface anticyclone located downstream of the upper-tropospheric ridge
419 over the western North Atlantic (Fig. 8b). The longitudinal juxtaposition of the surface cyclone
420 and anticyclone results in perturbation southerly geostrophic flow over eastern North America
421 and the subsequent poleward transport of anomalous precipitable water into the region. The
422 collocation of precipitable water anomalies and negative OLR anomalies in the vicinity of the
423 surface cyclone's warm-frontal boundary implies that widespread precipitation likely
424 accompanies the surface cyclone at this time. Diabatic heating associated with any implied areas
425 of precipitation subsequently contribute to the observed amplification of the upper-tropospheric
426 ridge over eastern North America during the following 24-h period (Figs. 8a,c).

427 24 h prior to superposition, 300-hPa geostrophic warm-air advection is diagnosed within
428 the entrance region of the developing superposed jet (Fig. 8c). The presence of geostrophic
429 warm-air advection suggests that the thermally-direct circulation within the jet-entrance region is
430 shifted poleward relative to the jet axis, positioning ascent directly beneath the jet core at this
431 time (e.g., Shapiro 1981, 1982; Lang and Martin 2012, 2013). Consequently, the surface cyclone
432 remains favorably located within a region of synoptic-scale ascent, which contributes to the
433 intensification of the surface cyclone during the previous 24-h period (Figs. 8b,d). The

intensification of both the surface cyclone and the downstream surface anticyclone compared to the prior time results in a strengthened zonal pressure gradient over eastern North America and intensified southerly geostrophic flow (Fig. 8d). This intensified southerly geostrophic flow leads to stronger poleward moisture transport and larger precipitable water anomalies within the surface cyclone's warm sector 24 h prior to superposition. The distribution of negative OLR anomalies at this time overlap the positions of the warm- and cold-frontal boundaries attendant to the surface cyclone (not shown), and the collocation of these OLR anomalies with anomalous moisture and implied ascent suggests that widespread precipitation persists on the equatorward side of the developing superposed jet.

The widespread precipitation and implied diabatic heating that accompany the surface cyclone contribute to further amplification of the upper-tropospheric ridge over eastern North America by the time of jet superposition (Figs. 8e,f). Consequently, the subtropical waveguide is displaced anomalously poleward of its climatological position, typical for a subtropical dominant event. While 300-hPa geostrophic warm-air advection persists along the jet axis at the time of superposition, areas of warm-air advection are now more focused in the jet-exit rather than in the jet-entrance region, as they were 24 h earlier (Figs. 8c,e). The presence of geostrophic warm-air advection in the jet-exit region suggests that the thermally-indirect circulation within the jet-exit region is shifted equatorward so as to promote continued ascent beneath the jet core (Fig. 8e). While the surface cyclone remains favorably aligned with this area of synoptic-scale ascent, the surface cyclone does not intensify during the 24-h period prior to superposition (Figs. 8d,f). Additionally, precipitable water anomalies and negative OLR anomalies have decreased in magnitude during the intervening 24-h period. Together, these observations imply that surface cyclogenesis and widespread precipitation tend to *lead* the development of eastern subtropical

457 dominant jet superpositions, in contrast to polar dominant events.

458 Farther upstream, 300-hPa geostrophic cold-air advection is diagnosed within the jet-
459 entrance region at the time of jet superposition (Fig. 8e). As discussed during polar dominant
460 events, geostrophic cold-air advection within the jet-entrance region is indicative of descent
461 beneath the jet core. This descent can subsequently act to restructure the tropopause and
462 contribute to the formation of the two-step tropopause structure that accompanies the jet
463 superposition. To investigate the formation of the superposed jet's two-step tropopause structure
464 further, a vertical cross section (D–D') is drawn immediately upstream of the jet superposition
465 centroid and perpendicular to the jet axis. The evolution of the tropopause is investigated within
466 this cross section both 12 h prior to superposition (Fig. 9a) and at the time of superposition (Fig.
467 9b).

468 Figure 9a depicts an area of ascent directly beneath the jet core 12 h prior to
469 superposition, consistent with the presence of geostrophic warm-air advection along the jet axis
470 and implied ascent along the surface cyclone's attendant frontal boundaries during the 24-h
471 period prior to superposition (Figs. 8c,d). This ascent accounts for a large fraction of the negative
472 PV advection diagnosed along the tropopause and acts to locally steepen the slope of the
473 tropopause during the 12-h period prior to superposition (Figs. 9a,b). Furthermore, given that this
474 ascent is occurring within an anomalously moist environment (Figs. 8d,f), diabatic heating likely
475 contributes to an erosion of upper-tropospheric PV on the equatorward side of the jet (Figs.
476 9a,b). In combination, these two processes reveal the direct role that moist ascent plays during
477 the production of eastern subtropical dominant superpositions through its contribution to the
478 development a tropopause structure that is considerably steeper by the time of superposition. A
479 narrow zone of descent also develops beneath the jet core at the time of superposition (Fig. 9b),

480 in agreement with the geostrophic cold-air advection diagnosed within the jet-entrance region
481 (Fig. 8e). As in polar dominant events, this descent facilitates the downward transport of high-
482 PV air from the lower stratosphere and contributes to the depth of the resultant two-step
483 tropopause structure that defines the jet superposition.

484 In contrast to polar dominant events (Figs. 7a,b), the cross sections shown in Figs. 9a,b
485 indicate that the superposed jet is characterized by the horizontal juxtaposition of a polar
486 cyclonic and a tropical anticyclonic PV anomaly during the 12-h period prior to superposition.
487 This configuration of upper-tropospheric PV anomalies strongly resembles the conceptual model
488 shown within Fig. 2 and indicates that the nondivergent circulations that accompany each PV
489 anomaly add constructively to produce the anomalously strong wind speeds associated with
490 eastern subtropical dominant jet superpositions. Consequently, knowledge of the creation,
491 transport towards midlatitudes, and phasing of these two types of PV anomalies is critical
492 towards correctly diagnosing the development of this jet superposition event type.

493 *c) Western Subtropical Dominant Events*

494 The development of western subtropical dominant events features the meridional
495 juxtaposition of an anomalous upper-tropospheric trough at high latitudes and an anomalous
496 ridge at subtropical latitudes 48 h prior to superposition, which results in a zonal extension of the
497 North Pacific jet stream (Fig. 10a). A surface cyclone is situated beneath the poleward-exit
498 region of the jet, and is characterized by a corridor of anomalous precipitable water within
499 perturbation southwesterly geostrophic flow on the cyclone's equatorward flank (Fig. 10b). The
500 aspect ratio of this corridor of anomalous precipitable water strongly resembles the character of
501 landfalling western U.S. atmospheric rivers (e.g., Newell et al. 1992; Zhu and Newell, 1998;
502 Ralph et al. 2004, 2018, 2019; Cannon et al. 2018), and is collocated with broad regions of 300-

503 hPa geostrophic warm-air advection and negative OLR anomalies. Consequently, the thermally-
504 indirect circulation within the jet-exit region favors synoptic-scale ascent and the production of
505 precipitation beneath the jet core in the vicinity of the Pacific Northwest at this time.
506 Perturbation geostrophic winds near the surface are also oriented perpendicular to the west coast
507 of North America, which suggests that orographic ascent likely contributes to the production of
508 precipitation during these events, as well.

509 Diabatic heating that accompanies any areas of implied ascent is primarily confined
510 equatorward of the developing superposed jet, suggesting that diabatic heating contributes to the
511 amplification of the eastern North Pacific ridge 24 h prior to superposition (Fig. 10c). The upper-
512 tropospheric trough poleward of the developing superposed jet also amplifies compared to the
513 prior time, which leads to the acceleration of a jet streak west of the North American continent.
514 The surface cyclone intensifies compared to the prior time beneath the poleward-exit region of
515 the developing superposed jet, and is characterized by a stronger and more spatially-coherent
516 corridor of anomalous precipitable water on its equatorward flank (Fig. 10d). The intersection of
517 anomalous precipitable water with negative OLR anomalies, stronger 300-hPa geostrophic
518 warm-air advection, and onshore lower-tropospheric geostrophic flow (Figs. 10c,d) suggests that
519 widespread precipitation persists along the west coast of North America on the equatorward side
520 of the developing superposed jet 24 h prior to superposition.

521 The perturbation upper-tropospheric trough and ridge near the west coast of North
522 America achieve their maximum intensity at the time of jet superposition, resulting in further
523 acceleration of wind speeds along the axis of the now superposed jet (Fig. 10e). The surface
524 cyclone remains within a favorable environment for synoptic-scale ascent beneath the poleward-
525 exit region of the superposed jet, with its corridor of anomalous precipitable water focused

farther south than at prior times along the central California coast (Figs. 10e,f). Negative OLR anomalies and sea level pressure anomalies decrease in magnitude, however, during the 24-h period prior to superposition (Figs. 10d,f). Similar to eastern subtropical dominant events, this observation suggests that surface cyclogenesis and widespread precipitation *lead* the formation of western subtropical dominant events.

As in polar and eastern subtropical dominant events, 300-hPa geostrophic cold-air advection develops within the entrance region of the jet at the time of superposition (Fig. 10e), indicating that the thermally-direct circulation in that location focuses descent beneath the jet core. To examine the impact of this descent as well as implied diabatic heating on the production of the jet's two-step tropopause structure, a cross section (E–E') is constructed immediately upstream of the jet superposition centroid and perpendicular to the jet axis. Figure 11a demonstrates that a focused region of ascent is present beneath the developing jet superposition 12 h prior to superposition, consistent with the presence of geostrophic warm-air advection along a considerable portion of the jet axis prior to superposition (Figs. 10c,e). This ascent accounts for a large fraction of the negative PV advection diagnosed along the tropopause and acts to locally steepen the tropopause. Additionally, given that this ascent is occurring within a corridor of anomalous moisture, diabatic heating that accompanies the ascent likely contributes to an erosion of upper-tropospheric PV on the equatorward side of the jet during the 12-h period prior superposition (Figs. 11a,b). The erosion of upper-tropospheric PV subsequently acts to further steepen the tropopause by the time of superposition.

A narrow zone of descent is diagnosed directly beneath the superposed jet core at the time of superposition (Fig. 11b). As in the previous event composites, this descent accounts for positive PV advection at the base of the tropopause break and, consequently, a downward

549 penetration of high-PV air from the lower stratosphere. The downward transport of high-PV air
550 from the lower stratosphere further steepens the tropopause and contributes to the formation of
551 the two-step tropopause structure that prevails at the time of superposition. Both cross sections
552 shown in Figs. 11a,b also demonstrate that the superposed jet is characterized by the meridional
553 juxtaposition of a polar cyclonic and tropical anticyclonic PV anomaly near the tropopause.
554 Consequently, the acceleration of wind speeds in the vicinity of the superposition results from
555 the constructive interference between the nondivergent circulations that accompany each PV
556 anomaly. Therefore, as in eastern subtropical dominant events, knowledge of the creation,
557 transport towards midlatitudes, and phasing of these two PV anomalies is critical for correctly
558 diagnosing the production of a western subtropical dominant event.
559
560 **5. Conclusion**
561 This study classifies North American jet superposition events into characteristic event
562 types based on the relative deviation of the polar and subtropical jets from their respective
563 climatological latitude bands, and investigates the dynamical mechanisms that facilitate the
564 production of a steep, two-step tropopause structure during each jet superposition event type.
565 The dynamical evolutions associated with each jet superposition event type are summarized
566 through a series of conceptual models presented in Fig. 12.
567 Polar dominant events (Fig. 12a) exhibit a preference for anticyclonic wave breaking
568 over the eastern North Pacific during the 48-h period prior to jet superposition. Anticyclonic
569 wave breaking subsequently facilitates the equatorward transport of a polar cyclonic PV anomaly
570 towards subtropical latitudes and allows the polar jet to superpose with the subtropical jet near
571 the climatological position of the subtropical jet. Surface cyclogenesis occurs primarily within

572 the poleward-exit region of the jet and peaks in intensity concurrently with the development of
573 the superposition. The surface cyclone features anomalous poleward moisture transport within its
574 warm sector, and is likely associated with widespread precipitation that also reaches peak
575 intensity and spatial coverage at the time of superposition. Given that surface cyclogenesis and
576 areas of implied precipitation are located well downstream of the jet superposition, moist ascent
577 and diabatic heating do not play a direct role in the formation of the two-step tropopause
578 structure that accompanies polar dominant events. Instead, upper-tropospheric geostrophic cold-
579 air advection within the entrance region of the developing superposed jet is indicative of descent
580 beneath the jet core. This descent is determined to play the primary role in facilitating the
581 development of the superposed jet's two-step tropopause structure during polar dominant events.
582 In contrast to polar dominant events, surface cyclogenesis and implied precipitation *lead*
583 the development of eastern subtropical dominant events (Fig. 12b). In particular, surface
584 cyclogenesis and implied precipitation occur predominantly within the equatorward-entrance
585 region of the developing superposed jet. Moist ascent, therefore, plays a direct role in the
586 development of the superposed jet's two-step tropopause structure by locally steepening the
587 tropopause via tilting and via the diabatic erosion of upper-tropospheric PV on the equatorward
588 side of the jet. As in polar dominant events, upper-tropospheric geostrophic cold-air advection
589 develops within the jet-entrance region during the 24-h period immediately preceding
590 superposition and indicates descent beneath the jet core in that location. This descent acts to
591 steepen the tropopause further by the time of superposition via the subduction of high-PV air
592 from the lower stratosphere, thereby completing the formation of the superposed jet's two-step
593 tropopause structure.

Western subtropical dominant events (Fig. 12c) are characterized by surface cyclogenesis that occurs beneath the poleward-exit region of the jet, rather than beneath the equatorward jet-entrance region as observed during eastern subtropical dominant events. The surface cyclone is accompanied by a zonally-oriented corridor of anomalous moisture that strongly resembles the character of a western U.S. atmospheric river. Widespread ascent and implied precipitation diagnosed along this corridor of anomalous moisture peak *prior* to the development of a jet superposition, as in eastern subtropical events, and play a direct role in the production of the superposed jet's two-step tropopause structure by steepening the tropopause locally via tilting and via the diabatic erosion of upper-tropospheric PV on the equatorward side of the jet. As observed during the other event types, upper-tropospheric geostrophic cold-air advection develops within the jet-entrance region by the time of superposition. Consequently, descent plays a critical role in completing the production of western subtropical dominant jet superpositions by contributing to the production of the superposed jet's two-step tropopause structure, as well.

The event types considered as part of this study reveal the varied roles that diabatic heating can play during the production of North American jet superpositions. Namely, surface cyclogenesis and implied precipitation appear to contribute directly to the formation of a two-step tropopause structure during subtropical dominant events, whereas surface cyclogenesis and implied precipitation develop concurrently with and downstream of polar dominant events. This difference motivates future work that investigates the relative importance of diabatic heating during observed jet superposition events. Of particular interest, is whether the omission of diabatic heating during the 48-h period prior to each jet superposition event type results in the successful formation of a jet superposition. It is hypothesized that subtropical dominant events are more sensitive to the omission of diabatic heating than polar dominant events, given the

617 direct role that diabatic heating appears to play in restructuring the tropopause during that event
618 type. The scrutiny of dry and full-physics simulations for select jet superposition events within
619 each event type is one pathway through which to examine in greater detail the role that diabatic
620 heating plays during jet superpositions.

621 A key result from this study is that descent beneath the entrance region of a developing
622 jet superposition is a shared element regardless of the event type under consideration. This result
623 motivates two critical research questions concerning the production of descent during jet
624 superposition events. First, what fraction of the observed descent is due to across-front
625 ageostrophic circulations that arise due to geostrophic frontogenesis within the confluent jet-
626 entrance region (i.e., divergence of the across-front component of the **Q**-vector) versus along-
627 front couplets of vertical motion that arise due to flow curvature and are of the scale of baroclinic
628 waves (i.e., divergence of the along-front component of the **Q**-vector; e.g., Keyser et al. 1992;
629 Martin 2006; Martin 2014)? The large-scale evolutions discussed in section 4 demonstrate that
630 both of these processes are certain to operate within North American jet superposition
631 environments. Second, what fraction of the observed descent within each event type can be
632 attributed to the three-dimensional circulations that accompany upper-tropospheric PV anomalies
633 along the polar and subtropical waveguides? The answer to the second question, in particular, is
634 likely to reveal the relative influence that polar cyclonic and tropical anticyclonic PV anomalies
635 have on the production of a superposed jet's two-step tropopause structure during each event
636 type, and, consequently, determine the degree to which superpositions result from midlatitude or
637 tropical dynamical processes.

638 North American jet superposition events during the cool season are most frequent during
639 November and December, rather than during January and February as they are in the western

640 North Pacific and northern Africa (Christenson et al. 2017; their Fig. 6). Given that North
641 American jet superpositions are generally preceded by the development of a high-amplitude flow
642 pattern, the frequency distribution of North American jet superposition events throughout the
643 cold season may be related to the lower frequency of Rossby wave breaking events in the eastern
644 North Pacific during the winter compared to the fall and spring (e.g., Abatzoglou and
645 Magnusdottir 2006; Bowley et al. 2019). Additionally, prior case study work suggests that jet
646 superpositions can form outside of the cold season (i.e., Christenson 2013; Winters and Martin
647 2014, 2016). Therefore, subsequent examinations of jet superposition events should modify the
648 jet identification scheme employed within this study to identify superposition events that occur
649 during the fall and spring. A comparison between jet superposition events across seasons has the
650 potential to highlight the degree to which the dynamical processes and the types of sensible
651 weather impacts that accompany jet superposition events vary as a function of season.

652 The composite analyses investigated in this study demonstrate that jet superpositions are
653 often associated with surface cyclogenesis, and a dynamical and thermodynamic environment
654 that is conducive to the production of widespread precipitation. However, a cursory examination
655 of individual events within each jet superposition event type indicates that some events are not
656 necessarily associated with sensible weather within the near-jet environment that can be
657 characterized as “high-impact”. Consequently, future work that differentiates between jet
658 superposition environments that lead to high-impact weather events versus those that result in
659 null events offers the potential to provide benefits to operational forecasts of high-impact
660 weather. Finally, the development and subsequent downstream propagation of superposed jets
661 can strongly reconfigure the large-scale flow pattern over the North Atlantic. Consequently,
662 further understanding of the impacts that North American jet superpositions may impose on the

663 downstream large-scale flow pattern may have important implications for operational forecasts
664 of conditions in western Europe.
665
666 *Acknowledgments*
667 This work was supported by the National Science Foundation through an AGS Postdoctoral
668 Research Fellowship (AGS-1624316) held at the University at Albany, SUNY by ACW.

669 **References**

670 Abatzoglou, J. T., and G. Magnusdottir, 2006: Planetary wave breaking and nonlinear reflection:
671 Seasonal cycle and interannual variability. *J. Climate*, **19**, 6139–6152,
672 doi: 10.1175/JCLI3968.1.

673 Agustí-Panareda, A., C. D. Thorncroft, G. C. Craig, and S. L. Gray, 2004: The extratropical
674 transition of Hurricane Irene (1999): A potential-vorticity perspective. *Quart. J. Roy.*
675 *Meteor. Soc.*, **130**, 1047–1074, doi: 10.1256/qj.02.140.

676 Ahmadi-Givi, F., G. C. Craig, and R. S. Plant, 2004: The dynamics of a midlatitude cyclone with
677 very strong latent-heat release. *Quart. J. Roy. Meteor. Soc.*, **130**, 295–323, doi:
678 10.1256/qj.02.226.

679 Archambault, H. M., L. F. Bosart, D. Keyser, and J. M. Cordeira, 2013: A climatological
680 analysis of the extratropical flow response to recurving western North Pacific tropical
681 cyclones. *Mon. Wea. Rev.*, **141**, 2325–2346, doi: 10.1175/MWR-D-12-00257.1.

682 Archambault, H. M., D. Keyser, L. F. Bosart, C. A. Davis, and J. M. Cordeira, 2015: A
683 composite perspective of the extratropical flow response to recurving western North
684 Pacific tropical cyclones. *Mon. Wea. Rev.*, **143**, 1122–1141, doi: 10.1175/MWR-D-14-
685 00270.1.

686 Bowley, K. A., J. R. Gyakum, and E. H. Atallah, 2019: A new perspective toward cataloging
687 Northern Hemisphere Rossby wave breaking on the dynamic tropopause. *Mon. Wea.*
688 *Rev.*, **147**, 409–431, doi: 10.1175/MWR-D-18-0131.1.

689 Cannon, F., C. W. Hecht, J. M. Cordeira, and F. M. Ralph, 2018: Synoptic and mesoscale forcing
690 of southern California extreme precipitation. *J. Geophys. Res.: Atmospheres*, **123**, 13714–
691 13730, doi: 10.1029/2018JD029045.

692 Cavallo, S. M., and G. J. Hakim, 2009: Potential vorticity diagnosis of a tropopause polar
693 cyclone. *Mon. Wea. Rev.*, **137**, 1358–1371, doi: 10.1175/2008MWR2670.1.
694 Cavallo, S. M., and G. J. Hakim, 2010: Composite structure of tropopause polar cyclones. *Mon.*
695 *Wea. Rev.*, **138**, 3840–3857, doi: 10.1175/2010MWR3371.1.
696 Cavallo, S. M., and G. J. Hakim, 2012: Radiative impact on tropopause polar vortices over the
697 Arctic. *Mon. Wea. Rev.*, **140**, 1683–1702, doi: 10.1175/MWR-D-11-00182.1.
698 Cavallo, S. M., and G. J. Hakim, 2013: Physical mechanisms of tropopause polar vortex intensity
699 change. *J. Atmos. Sci.*, **70**, 3359–3373, doi: 10.1175/JAS-D-13-088.1.
700 Christenson, C. E., 2013: A synoptic-climatology of Northern Hemisphere polar and subtropical
701 jet superposition events. M.S. thesis, University of Wisconsin–Madison, 62 pp.
702 Christenson, C. E., J. E. Martin, Z. J. Handlos, 2017: A synoptic climatology of Northern
703 Hemisphere, cold season polar and subtropical jet superposition events. *J. Climate*, **30**,
704 7231–7246, doi: 10.1175/JCLI-D-16-0565.1.
705 Defant, F., and H. Taba, 1957: The threefold structure of the atmosphere and the characteristics
706 of the tropopause. *Tellus,* **9**, 259–275, doi:10.3402/tellusa.v9i3.9112.
707 Fröhlich, L., P. Knippertz, A. H. Fink, and E. Hohberger, 2013: An objective climatology of
708 tropical plumes. *J. Climate*, **26**, 5044–5060, doi: 10.1175/JCLI-D-12-00351.1.
709 Grams, C. M., H. Wernli, M. Böttcher, J. Čampa, U. Corsmeier, S. C. Jones, J. H. Keller, C.-J.
710 Lenz, and L. Wiegand, 2011: The key role of diabatic processes in modifying the upper-
711 tropospheric wave guide: A North Atlantic case-study. *Quart. J. Roy. Meteor. Soc.*, **137,**
712 2174–2193, doi: 10.1002/qj.891.
713 Grams, C. M., S. C. Jones, C. A. Davis, P. A. Harr, and M. Weissmann, 2013: The impact of
714 Typhoon Jangmi (2008) on the midlatitude flow. Part I: Upper-level ridgebuilding and

715 modification of the jet. *Quart. J. Roy. Meteor. Soc.,* **139,** 2148−2164, doi:
716 10.1002/qj.2091.
717 Grams, C. M., H. M. Archambault, 2016: The key role of diabatic outflow in amplifying the
718 midlatitude flow: A representative case study of weather systems surrounding western
719 North Pacific extratropical transition. *Mon. Wea. Rev.*, **144**, 3847–3869, doi:
720 10.1175/MWR-D-15-0419.1.
721 Hakim, G. J., 2000: Climatology of coherent structures on the extratropical tropopause. *Mon.*
722 *Wea. Rev.*, **128**, 385–406, doi: 10.1175/1520-
723 0493%282000%29128<0385%3ACOCSOT>2.0.CO%3B2.
724 Hakim, G. J., L. F. Bosart, and D. Keyser, 1995: The Ohio Valley wave-merger cyclogenesis
725 event of 25–26 January 1978. Part I: Multiscale case study. *Mon. Wea. Rev.*, **123**, 2663–
726 2692, doi: 10.1175/1520-0493(1995)123<2663:TOVWMC>2.0.CO;2.
727 Hakim, G. J., D. Keyser, and L. F. Bosart, 1996: The Ohio Valley wave-merger cyclogenesis
728 event of 25–26 January 1978. Part II: Diagnosis using quasigeostrophic potential vorticity
729 inversion. *Mon. Wea. Rev.*, **124**, 2176–2205, doi: 10.1175/1520-
730 0493(1996)124<2176:TOVWMC>2.0.CO;2.
731 Handlos, Z. J., and J. E. Martin, 2016: Composite analysis of large-scale environments
732 conducive to west Pacific polar/subtropical jet superposition. *J. Climate*, **29**, 7145–7165,
733 doi: 10.1175/JCLI-D-16-0044.1.
734 Held, I. M., 1975: Momentum transport by quasi-geostrophic eddies. *J. Atmos. Sci.*, **32**, 1494–
735 1497, doi: 10.1175/ 1520-0469(1975)032,1494:MTBQGE.2.0.CO;2.

736 Held, I. M., and A. Y. Hou, 1980: Nonlinear axially symmetric circulations in a nearly inviscid
737 atmosphere. *J. Atmos. Sci.*, **37**, 515–533, doi: 10.1175/1520-
738 0469(1980)037<0515:NASCIA>2.0.CO;2.
739 Iskenderian, H., 1995: A 10-year climatology of Northern Hemisphere tropical cloud plumes and
740 their composite flow patterns. *J. Climate*, **8**, 1630–1637, doi: 10.1175/1520-
741 0442(1995)008<1630:AYCONH>2.0.CO;2.
742 Kalnay, E., and Coauthors, 1996: The NCEP/NCAR 40-Year Reanalysis Project. *Bull. Amer.*
743 *Meteor. Soc.*, **77**, 437–470, doi: 10.1175/1520-0477(1996)077,0437:TNYRP.2.0.CO;2.
744 Keyser, D., and M. J. Pecnick, 1985: A two-dimensional primitive equation model of
745 frontogenesis forced by confluence and horizontal shear. *J. Atmos. Sci.*, **42**, 1259–1282,
746 doi: 10.1175/1520-0469(1985)042,1259:ATDPEM.2.0.CO;2.
747 Keyser, D., and M. A. Shapiro, 1986: A review of the structure and dynamics of upper-level
748 frontal zones. *Mon. Wea. Rev.*, **114**, 452–499, doi: 10.1175/1520-
749 0493(1986)114<0452:AROTSA>2.0.CO;2.
750 Keyser, D., B. D. Schmidt, and D. G. Duffy, 1992: Quasigeostrophic vertical motions diagnosed
751 from along- and cross-isentrope components of the Q vector. *Mon. Wea. Rev.*, **120**, 731–
752 741, doi: 10.1175/1520-0493%281992%29120<0731%3AQVMDFA>2.0.CO%3B2.
753 Kistler, R., and Coauthors, 2001: The NCEP–NCAR 50-Year Reanalysis: Monthly means CD-
754 ROM and documentation. *Bull. Amer. Meteor. Soc.*, **82**, 247–267, doi: 10.1175/ 1520-
755 0477(2001)082,0247:TNNYRM.2.3.CO;2.
756 Koteswaram, P., 1953: An analysis of the high tropospheric wind circulation over India in
757 winter. *Indian J. Meteor. Geophys.*, **4**, 13–21.

758 Koteswaram, P., and S. Parthasarathy, 1954: The mean jet stream over Indian in the pre-
759 monsoon and post-monsoon seasons and vertical motions associated with subtropical jet
760 streams. *Indian J. Meteor. Geophys.*, **5**, 138–156.
761 Krishnamurti, T. N., 1961: The subtropical jet stream of winter. *J. Meteor.*, **18**, 172–191, doi:
762 10.1175/1520-0469(1961)018<0172:TSJSOW>2.0.CO;2.
763 Lang, A. A., and J. E. Martin, 2012: The structure and evolution of lower stratospheric frontal
764 zones. Part I: Examples in northwesterly and southwesterly flow. *Quart. J. Roy. Meteor.*
765 *Soc.*, **138**, 1350–1365, doi: 10.1002/qj.843.
766 Lang, A. A., and J. E. Martin, 2013: The structure and evolution of lower stratospheric frontal
767 zones: Part II: The influence of tropospheric ascent on lower stratospheric frontal
768 development. *Quart. J. Roy. Meteor. Soc.*, **139**, 1798–1809, doi: 10.1002/qj.2074.
769 Lee, S., and H.-K. Kim, 2003: The dynamical relationship between subtropical and eddy-driven
770 jets. *J. Atmos. Sci.*, **60**, 1490–1503, doi: 10.1175/1520-
771 0469%282003%29060<1490%3ATDRBSA>2.0.CO%3B2.
772 Liebmann, B., and C. A. Smith, 1996: Description of a complete (interpolated) outgoing
773 longwave radiation dataset. *Bull. Amer. Meteor. Soc.*, **77**, 1275–1277.
774 Loewe, F., and V. Radok, 1950: A meridional aerological cross section in the southwest
775 Pacific. *J. Meteor.*, **7**, 58–65, doi: 10.1175/1520-
776 0469(1950)007<0058:AMACSI>2.0.CO;2.
777 Martin J. E., 2006. The role of shearwise and transverse quasigeostrophic vertical motions in the
778 midlatitude cyclone life cycle. *Mon. Wea. Rev*., **134**, 1174–1193, doi:
779 10.1175/MWR3114.1.

780 Martin, J. E., 2014: Quasi-geostrophic diagnosis of the influence of vorticity advection on the
781 development of upper level jet-front systems. *Quart. J. Roy. Meteor. Soc.*, **140**, 2658–
782 2671, doi: 10.1002/qj.2333.
783 Martius, O., C. Schwiertz, and H. C. Davies, 2010: Tropopause-level waveguides. *J. Atmos.*
784 *Sci.*, **67**, 866–879, doi: 10.1175/2009JAS2995.1.
785 McTaggart-Cowan, R., J. R. Gyakum, and M. K. Yau, 2001: Sensitivity testing of extratropical
786 transitions using potential vorticity inversions to modify initial conditions: Hurricane Earl
787 case study. *Mon. Wea. Rev.*, **129**, 1617–1636, doi: 10.1175/1520-
788 0493%282001%29129<1617%3ASTOETU>2.0.CO%3B2.
789 McTaggart-Cowan, R., J. R. Gyakum, and M. K. Yau, 2004: The impact of tropical remnants on
790 extratropical cyclogenesis: Case study of Hurricanes Danielle and Earl (1998). *Mon.*
791 *Wea. Rev.*, **132**, 1933–1951, doi: 10.1175/1520-
792 0493%282004%29132<1933%3ATIOTRO>2.0.CO%3B2.
793 McTaggart-Cowan, R., L. F. Bosart, J. R. Gyakum, and E. H. Atallah, 2007: Hurricane Katrina
794 (2005). Part II: Evolution and hemispheric impacts of a diabatically generated warm pool.
795 *Mon. Wea. Rev.*, **135**, 3927–3949, doi: 10.1175/2007MWR2096.1.
796 McWilliams, J. C., and J. H. S. Chow, 1981: Equilibrium geostrophic turbulence I: Reference
797 solution in a b-plane channel. *J. Phys. Oceanogr.*, **11**, 921–949, doi: 10.1175/1520-
798 0485(1981)011,0921:EGTIAR.2.0.CO;2.
799 Mohri, K., 1953: On the fields of wind and temperature over Japan and adjacent waters during
800 winter of 1950–1951. *Tellus*, **5**, 340–358, doi: 10.3402/tellusa.v5i3.8582.
801 Namias, J., and P. F. Clapp, 1949: Confluence theory of the high tropospheric jet stream. *J.*
802 *Meteor.*, **6**, 330–336, doi: 10.1175/1520-0469(1949)006<0330:CTOTHT>2.0.CO;2.

Newell, R. E., N. E. Newell, Y. Zhu, and C. Scott, 1992: Tropospheric rivers?—A pilot study. *Geophys. Res. Lett.*, **19**, 2401–2404, doi: 10.1029/92GL02916.

Newton, C. W., 1954: Frontogenesis and frontolysis as a three-dimensional process. *J. Meteor.*, **11**, 449–461, doi: 10.1175/1520-0469(1954)011<0449:FAFAAT>2.0.CO;2.

Palmén, E., and C. W. Newton, 1948: A study of the mean wind and temperature distribution in the vicinity of the polar front in winter. *J. Meteor.*, **5**, 220–226, doi: 10.1175/1520-0469(1948)005<0220:ASOTMW>2.0.CO;2.

Palmén, E., and C. W. Newton, 1969: *Atmospheric Circulation Systems: Their Structure and Physical Interpretation*. Academic Press, 603 pp.

Panetta, R. L., 1993: Zonal jets in wide baroclinically unstable regions: Persistence and scale selection. *J. Atmos. Sci.*, **50**, 2073–2106, doi: 10.1175/1520-0469(1993)050,2073:ZJIWBU.2.0.CO;2.

Pyle, M. E., D. Keyser, and L. F. Bosart, 2004: A diagnostic study of jet streaks: Kinematic signatures and relationship to coherent tropopause disturbances. *Mon. Wea. Rev.*, **132**, 297–319, doi: 10.1175/1520-0493(2004)132<0297:ADSOJS>2.0.CO;2.

Ralph, F. M., P. J. Neiman, and G. A. Wick, 2004: Satellite and CALJET aircraft observations of atmospheric rivers over the eastern North Pacific Ocean during the winter of 1997/98. *Mon. Wea. Rev.*, **132**, 1721–1745, doi: 10.1175/1520-0493(2004)132<1721:SACAOO>2.0.CO;2.

Ralph, F. M., M. D. Dettinger, M. M. Cairns, T. J. Galarneau, and J. Eylander, 2018: Defining "atmospheric river": How the *Glossary of Meteorology* helped resolve a debate. *Bull. Amer. Meteor. Soc.*, **99**, 837–839, doi: 10.1175/BAMS-D-17-0157.1

825 Ralph, F. M., and Coauthors, 2019: A scale to characterize the strength of impacts of
826 atmospheric rivers. *Bull. Amer. Meteor. Soc.*, **100**, 269–289, doi: 10.1175/BAMS-D-18-
827 0023.1.
828 Rhines, P. B., 1975: Waves and turbulence on a beta-plane. *J. Fluid Mech.*, **69**, 417–433, doi:
829 10.1017/S0022112075001504.
830 Riehl, H., 1962: Jet streams of the atmosphere. Dept. of Atmospheric Science Tech. Rep. 32,
831 Colorado State University, Fort Collins, CO, 117 pp.
832 Rotunno, R., W. C. Skamarock, and C. Snyder, 1994: An analysis of frontogenesis in numerical
833 simulations of baroclinic waves. *J. Atmos. Sci.*, **51**, 3373–3398, doi: 10.1175/1520-
834 0469(1994)051,3373:AAOFIN.2.0.CO;2
835 Roundy, P. E., K. MacRitchie, J. Asuma, and T. Melino, 2010: Modulation of the global
836 atmospheric circulation by combined activity in the Madden–Julian oscillation and the El
837 Niño–Southern Oscillation during boreal winter. *J. Climate*, **23**, 4045–4059, doi:
838 10.1175/2010JCLI3446.1.
839 Saha, S., and Coauthors, 2010: The NCEP Climate Forecast System Reanalysis. *Bull. Amer.*
840 *Meteor. Soc.*, **91**, 1015–1057, doi: 10.1175/2010BAMS3001.1.
841 Schultz, D. M., and C. A. Doswell III, 1999: Conceptual models of upperlevel frontogenesis in
842 south-westerly and north-westerly flow. *Quart. J. Roy. Meteor. Soc.*, **125**, 2535–2562,
843 doi: 10.1002/qj.49712555910.
844 Schultz, D. M., and F. Sanders, 2002: Upper-level frontogenesis associated with the birth of
845 mobile troughs in northwesterly flow. *Mon. Wea. Rev.*, **130**, 2593–2610, doi:
846 10.1175/1520-0493 (2002)130,2593:ULFAWT.2.0.CO;2.

847 Shapiro, M. A., 1981: Frontogenesis and geostrophically forced secondary circulations in the
848 vicinity of jet stream-frontal zone systems. *J. Atmos. Sci.*, **38**, 954–973, doi:
849 10.1175/1520-0469(1981)038<0954:FAGFSC>2.0.CO;2.
850 Shapiro, M. A., 1982: *Mesoscale weather systems of the central United States.* CIRES, 78 pp.
851 Shapiro, M. A., T. Hampel, and A. J. Krueger, 1987: The Arctic tropopause fold. *Mon. Wea.*
852 *Rev.*, **115**, 444–454, doi: 10.1175/1520-0493(1987)115,0444:TATF.2.0.CO;2.
853 Shapiro, M. A., and D. Keyser, 1990: Fronts, jet streams, and the tropopause. *Extratropical*
854 *Cyclones: The Erik Palmén Memorial Volume*, C. Newton and E. O. Holopainen, Eds.,
855 Amer. Meteor. Soc., 167–191.
856 Son, S.-W., and S. Lee, 2005: The response of westerly jets to thermal driving in a primitive
857 equation model. *J. Atmos. Sci.*, **62**, 3741–3757, doi: 10.1175/JAS3571.1.
858 Sutcliffe, R. C., and J. K. Bannon, 1954: Seasonal changes in the upper-air conditions in the
859 Mediterranean Middle East area. *Proc. Int. Association of Meteorology*, Rome, Italy, Int.
860 Union of Geodesy and Geophysics. 322–334.
861 Wilks, D. S., 2011: Statistical Methods in the Atmospheric Sciences. 3rd ed. Elsevier, 676 pp.
862 Winters, A. C., and J. E. Martin, 2014: The role of a polar/subtropical jet superposition in the
863 May 2010 Nashville flood. *Wea. Forecasting*, **29**, 954–974, doi: 10.1175/WAF-D-13-
864 00124.1.
865 Winters, A. C., and J. E. Martin, 2016: Synoptic and mesoscale processes supporting vertical
866 superposition of the polar and subtropical jets in two contrasting cases. *Quart. J. Roy.*
867 *Meteor. Soc.*, **142**, 1133–1149, doi: 10.1002/qj.2718.

Winters, A. C., and J. E. Martin, 2017: Diagnosis of a North American polar–subtropical jet superposition employing piecewise potential vorticity inversion. *Mon. Wea. Rev.*, **145**, 1853–1873, doi: 10.1175/MWR-D-16-0262.1.

Yeh, T. C., 1950: The circulation of the high tropopause over China in the winter of 1945–46. *Tellus*, **2**, 173–183, doi: 10.3402/tellusa.v2i3.8548.

Zhu, Y., and R. E. Newell, 1998: A proposed algorithm for moisture fluxes from atmospheric rivers. *Mon. Wea. Rev.*, **126**, 725–735, doi: 10.1175/1520-0493(1998)126<0725:APAFMF>2.0.CO;2.

Tables

Jet Superposition Characteristics				
	Avg. Starting Latitude	Avg. Starting Longitude	Avg. ΔLatitude	Avg. ΔLongitude
Polar Dominant (N = 80)	29.7°N	102.0°W	+3.42°	+12.25°
Hybrid (N=117)	34.5°N	94.3°W	+0.85°	+11.20°
Subtropical Dominant (N=129)	46.7°N	92.1°W	–0.96°	+12.32°
East Subtropical Dominant (N=76)	48.5°N	71.2°W	–1.13°	+9.56°
West Subtropical Dominant (N=53)	44.0°N	122.1°W	–0.78°	+15.10°

TABLE 1. Average characteristics of jet superposition events as a function of event type. These characteristics include the average latitude and longitude at which jet superpositions develop for each event type, and the average change (Δ) in latitude and longitude a jet superposition's position during its lifespan for each event type.

Figures

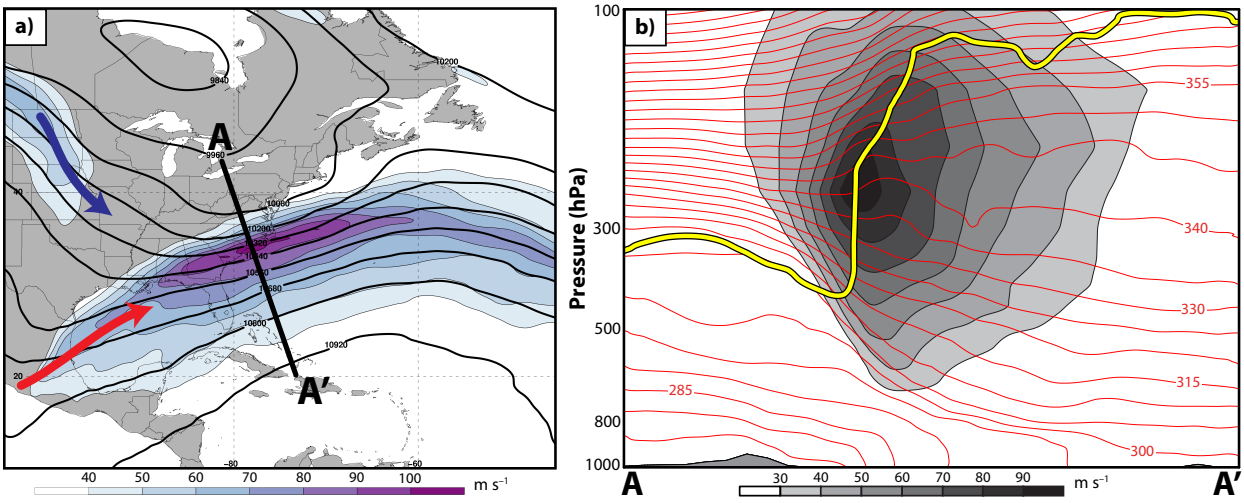

FIG. 1. (a) 250-hPa geopotential height is contoured in black every 120 m and 250-hPa wind speed is shaded in m s^{-1} according the legend at 1200 UTC 20 December 2009. The blue and red arrows identify flow along the polar and subtropical waveguides, respectively. (b) Cross section from A–A', as indicated in (a), of a jet superposition. Wind speed is shaded in m s^{-1} according the legend, potential temperature is contoured in red every 5 K, and the 2-PVU contour is drawn in yellow to highlight the structure of the dynamic tropopause.

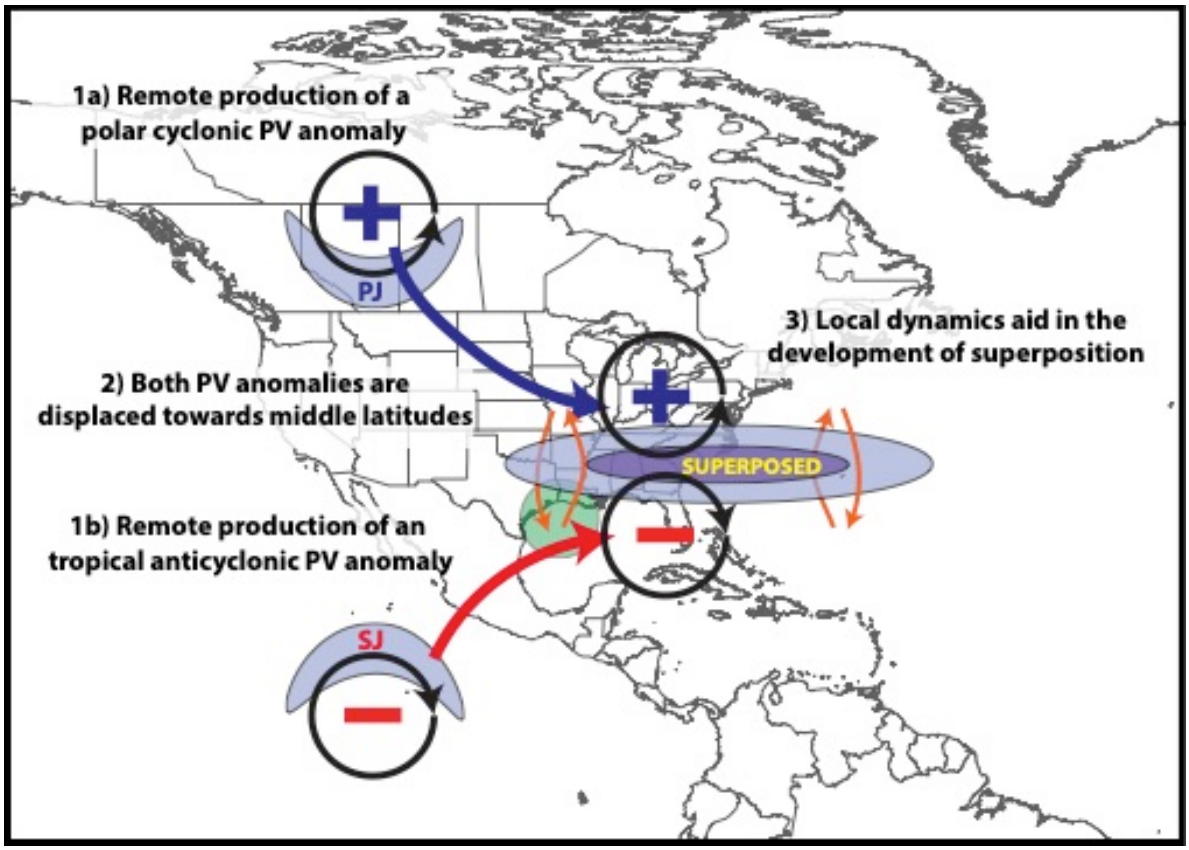

FIG. 2. Conceptual diagram summarizing the development of a jet superposition. The orange arrows depict the branches of an across-front ageostrophic circulation, the green circle identifies an area of convection, and the plus (minus) sign corresponds to the center of a polar cyclonic (tropical anticyclonic) PV anomaly, with the blue (red) arrow indicating the movement of that particular PV anomaly toward midlatitudes. The purple fill pattern corresponds to isotachs, with the darker shade of purple identifying faster wind speeds. The locations of the polar jet (PJ), subtropical jet (SJ), and superposed jet are labeled accordingly. Figure and caption adapted from Winters and Martin (2017).

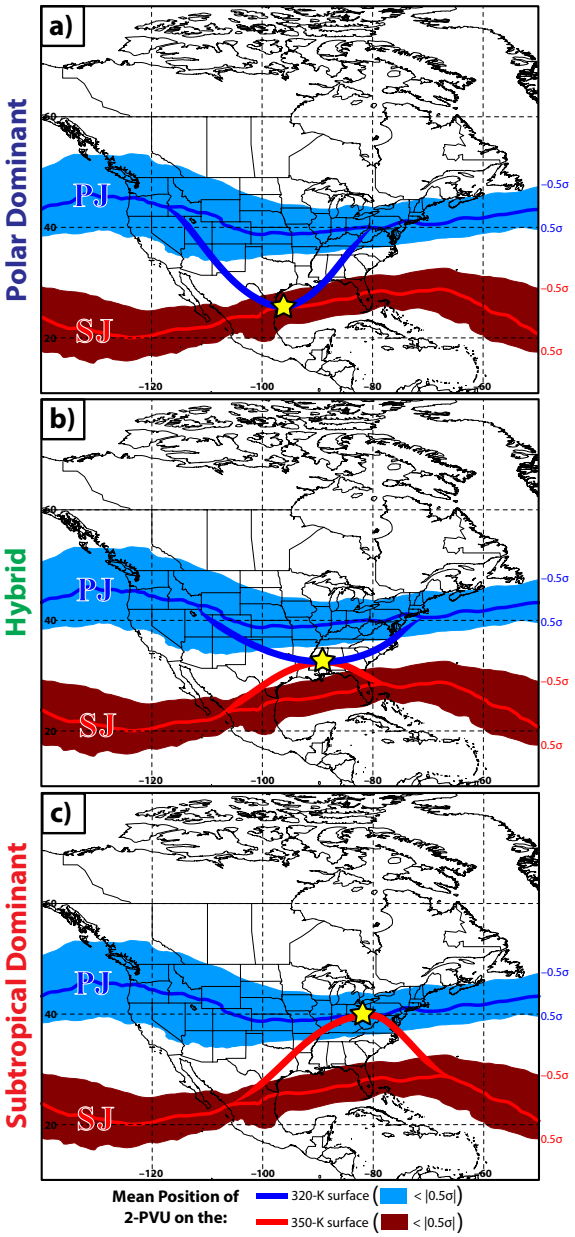

FIG. 3. The mean position of the 2-PVU contour on the 320-K and 350-K isentropic surfaces at 0000 UTC 1 January is indicated by the thin blue and red line, respectively, and represents the mean position of the polar (PJ) and subtropical (SJ) waveguides. Shaded areas bounding each mean 2-PVU contour indicate locations at which an observation of 2-PVU on that particular isentropic surface would represent a standardized PV anomaly with a magnitude less than 0.5. Hypothetical deviations of the 2-PVU contour from its mean position on each isentropic surface that result in the formation of (a) a polar dominant jet superposition event (yellow star) are indicated by the thick blue and red contours. (b) As in (a), but for a hybrid event. (c) As in (a), but for a subtropical dominant event.

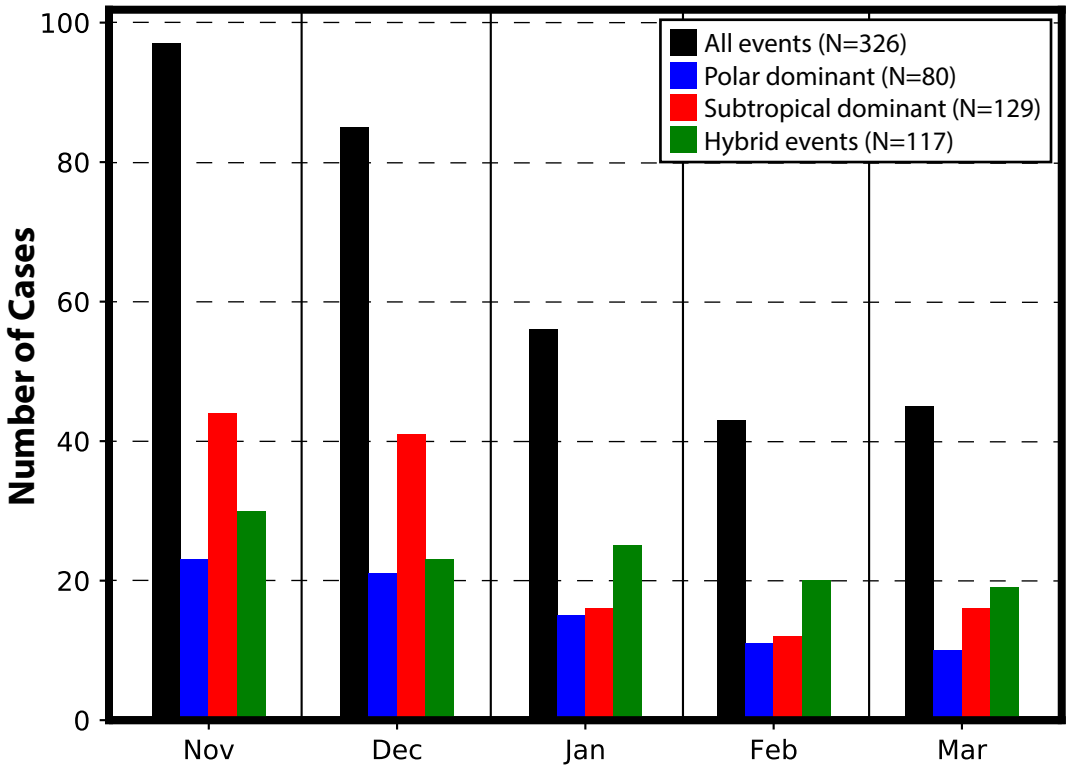

916
917 FIG. 4. Monthly frequency of jet superposition events as a function of event type.
918

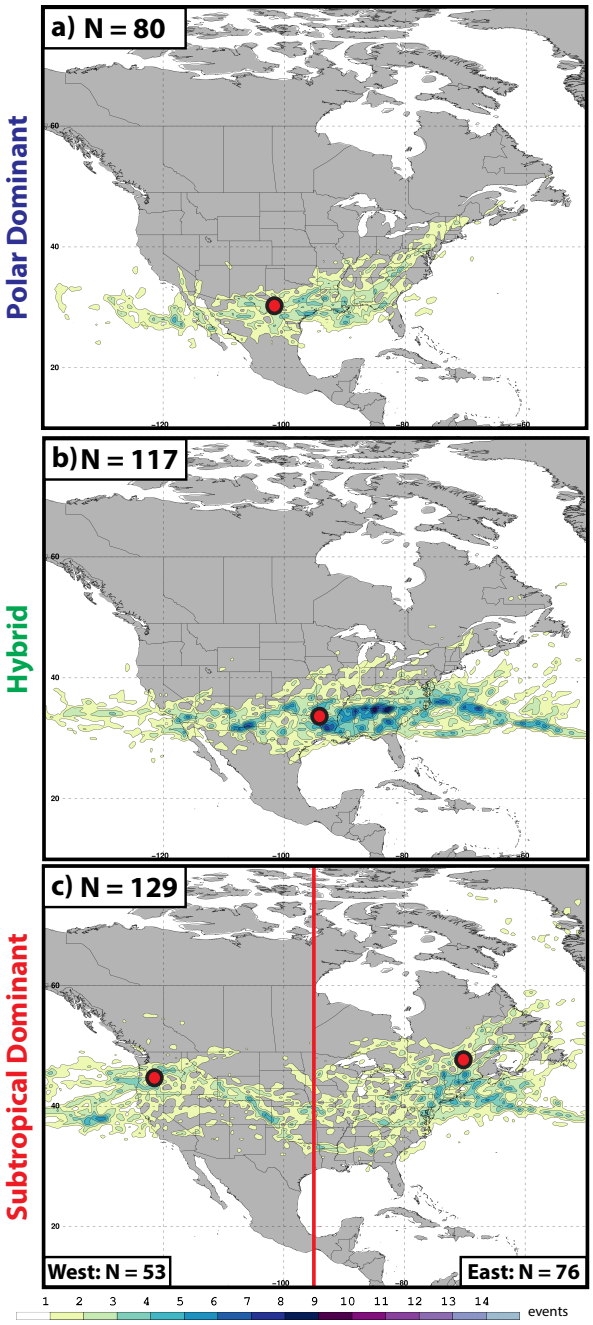

FIG. 5. (a) The spatial frequency of polar dominant jet superposition events is shaded following the legend. The red circle represents the average location of jet superposition for polar dominant events, as indicated in Table 1. (b) As in (a), but for hybrid events. (c) As in (a) but for subtropical dominant events. The vertical red bar in (c) is used to illustrate the partition of subtropical dominant events into an eastern and a western category. The red dot to the east (west) of the vertical red line in (c) indicates the average location of superposition for eastern (western) subtropical dominant events.

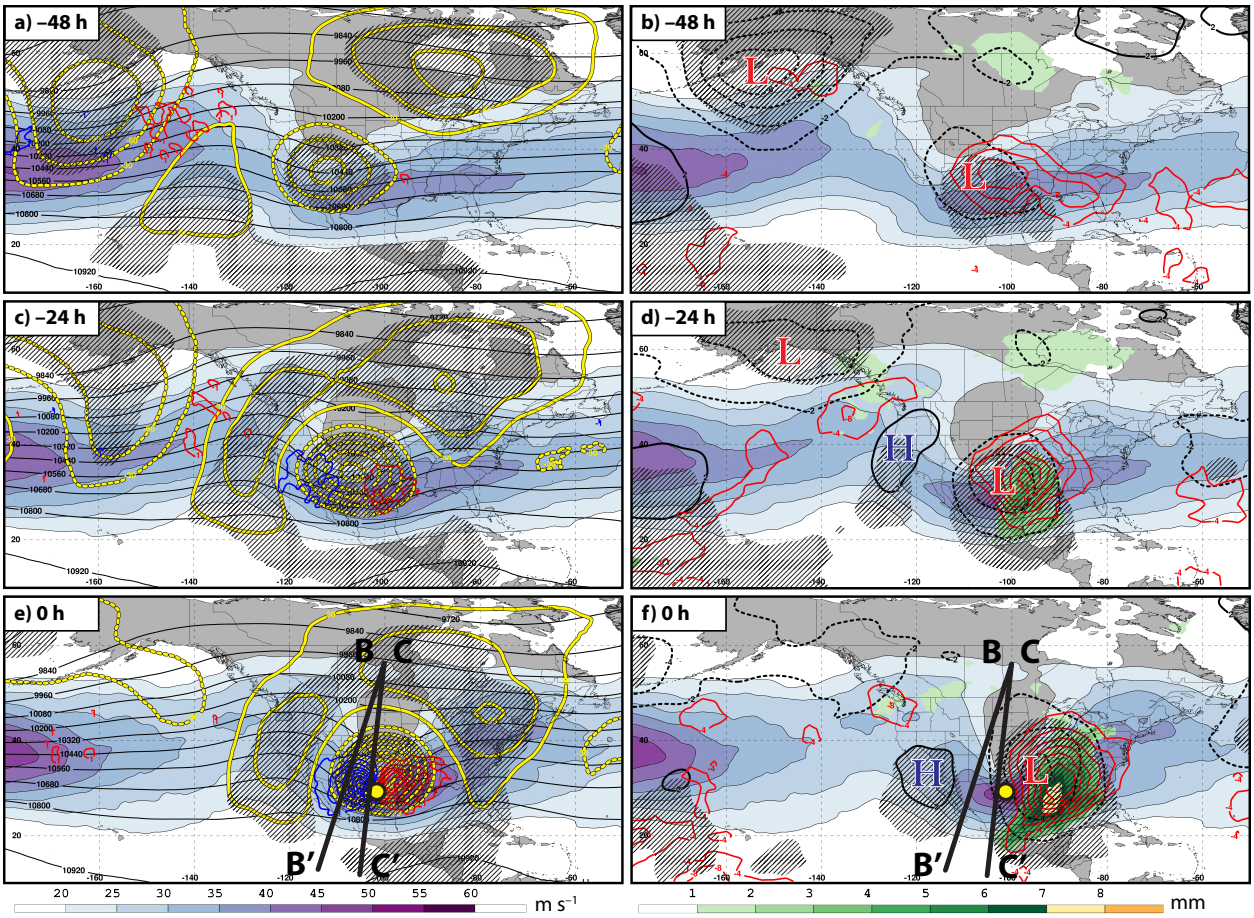

FIG. 6. Composite large-scale flow evolution prior to the initiation of a polar dominant jet superposition event. (left) 250-hPa geopotential height is contoured in black every 120 m, 250-hPa geopotential height anomalies are contoured in solid and dashed yellow every 30 m for positive and negative values, respectively, 250-hPa wind speed is shaded in m s^{-1} according to the legend, and 300-hPa geostrophic cold- (warm-) air advection is contoured in blue (red) every 1×10^{-4} K s^{-1} for (a) 48 h, (c) 24 h, and (e) 0 h prior to jet superposition. Hatched areas represent locations where the 250-hPa geopotential height anomalies are statistically distinct from climatology at the 99% confidence level. (right) 250-hPa wind speed is shaded in m s^{-1} according the legend, mean sea level pressure anomalies are contoured in solid and dashed black every 2 hPa for positive and negative values, respectively, negative OLR anomalies are contoured in red every 4 W m^{-2}, and precipitable water anomalies are shaded in mm according to legend at locations in which they are statistically distinct from climatology at the 99% confidence level for (b) 48 h, (d) 24 h, and (f) 0 h prior to jet superposition. Hatched areas represent locations where the mean sea level pressure anomalies are statistically distinct from climatology at the 99% confidence level. The red "L"s and blue "H"s identify the locations of surface cyclones and anticyclones.

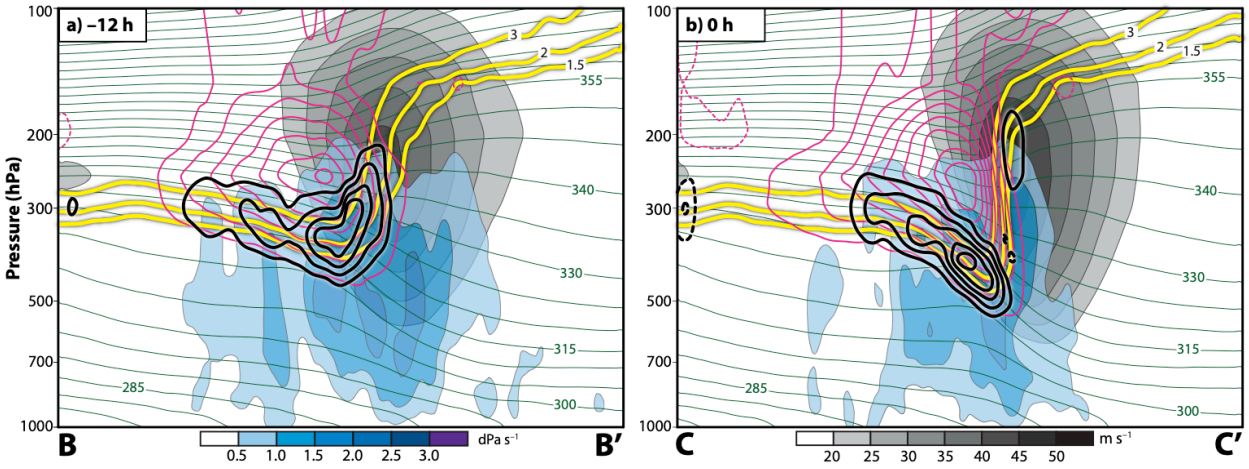

FIG. 7. (a) Cross section from B–B', as indicated in Figs. 6e,f, 12 h prior to a polar dominant jet superposition event. Potential temperature is contoured in green every 5 K, wind speed (m s^{-1}) is shaded in grey according the legend, positive (negative) PV anomalies are contoured in solid (dashed) magenta contours every 0.5 PVU, the 1.5, 2-, and 3-PVU contours are indicated in yellow, positive (negative) PV advection accomplished by the divergent wind is contoured in solid (dashed) black contours every 0.5×10^{-5} PVU s^{-1}, and descent (dPa s^{-1}) is shaded in blue according the legend. (b) As in (a), but for the cross section from C–C', as indicated in Figs. 6e,f, 0 h prior to a polar dominant jet superposition event.

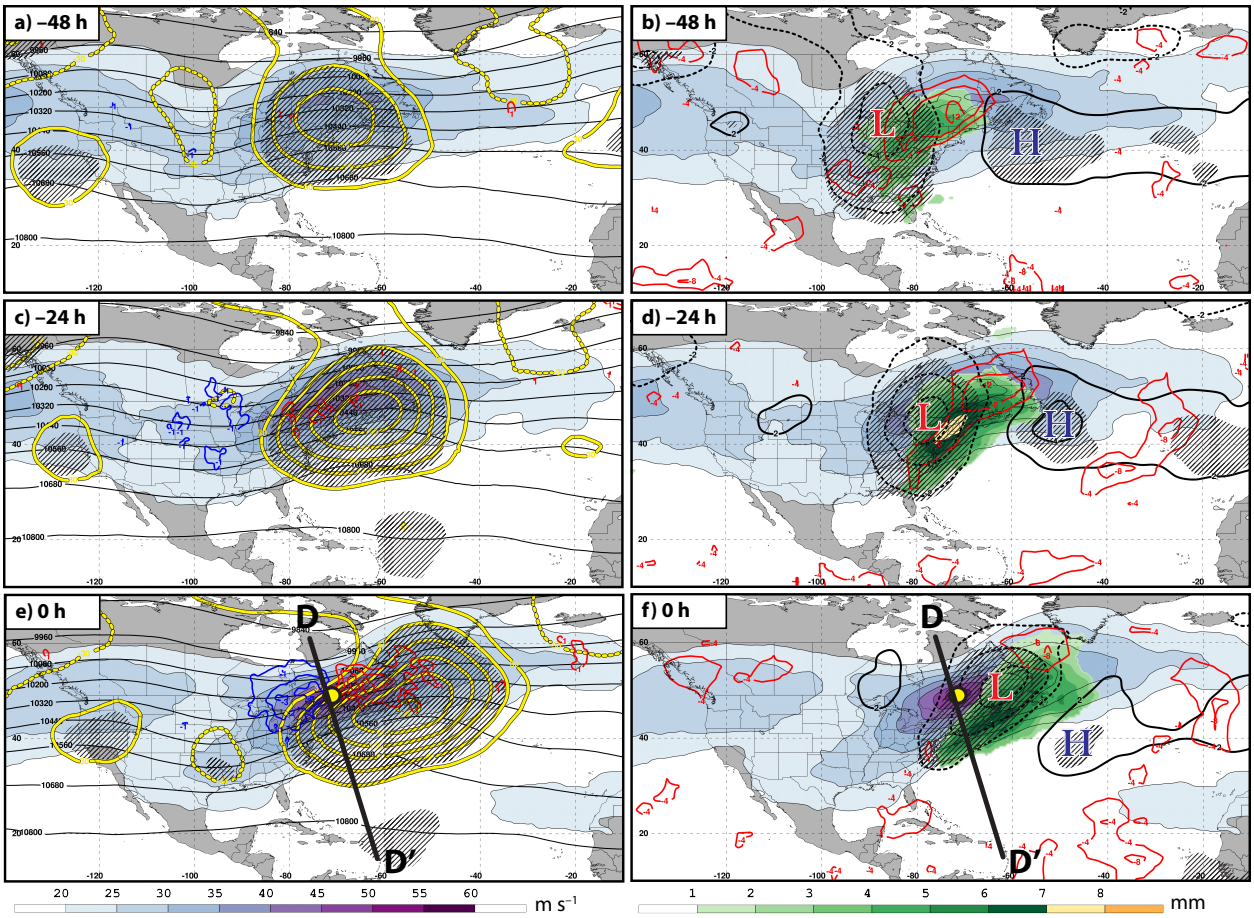

FIG. 8. Composite large-scale flow evolution prior to the initiation of an eastern subtropical dominant jet superposition event. All conventions are identical to those in Fig. 6.

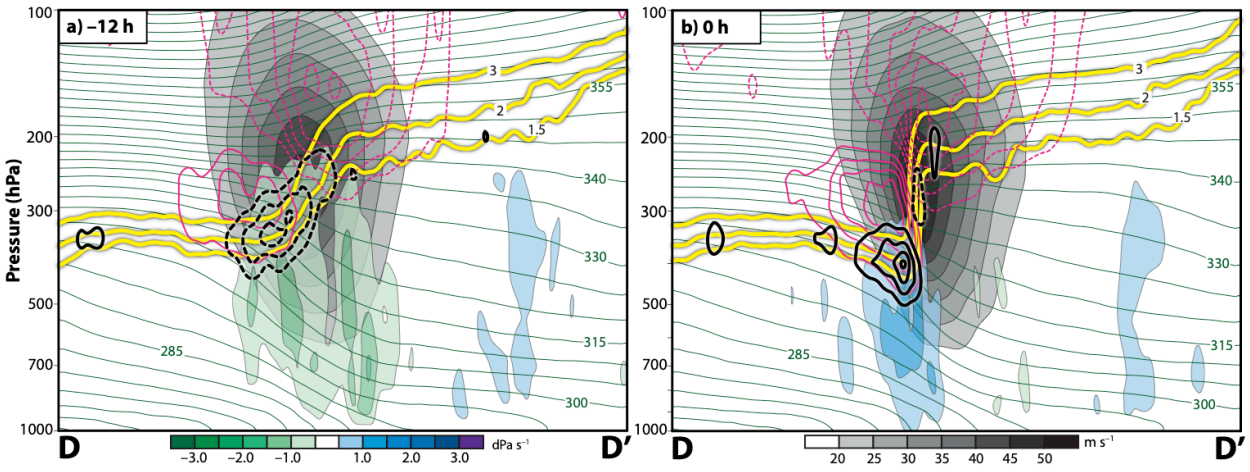

FIG. 9. (a) Cross section from D–D', as indicated in Figs. 8e,f, 12 h prior to an eastern subtropical dominant jet superposition event. Potential temperature is contoured in green every 5 K, wind speed (m s^{-1}) is shaded in grey according the legend, positive (negative) PV anomalies are contoured in solid (dashed) magenta contours every 0.5 PVU, the 1.5, 2-, and 3-PVU contours are indicated in yellow, positive (negative) PV advection accomplished by the divergent wind is contoured in solid (dashed) black contours every 0.5×10^{-5} PVU s^{-1}, and vertical motion (dPa s^{-1}) is shaded in blue and green according the legend for descent and ascent, respectively. (b) As in (a), but for the cross section from D–D', as indicated in Figs. 8e,f, 0 h prior to an eastern subtropical dominant jet superposition event.

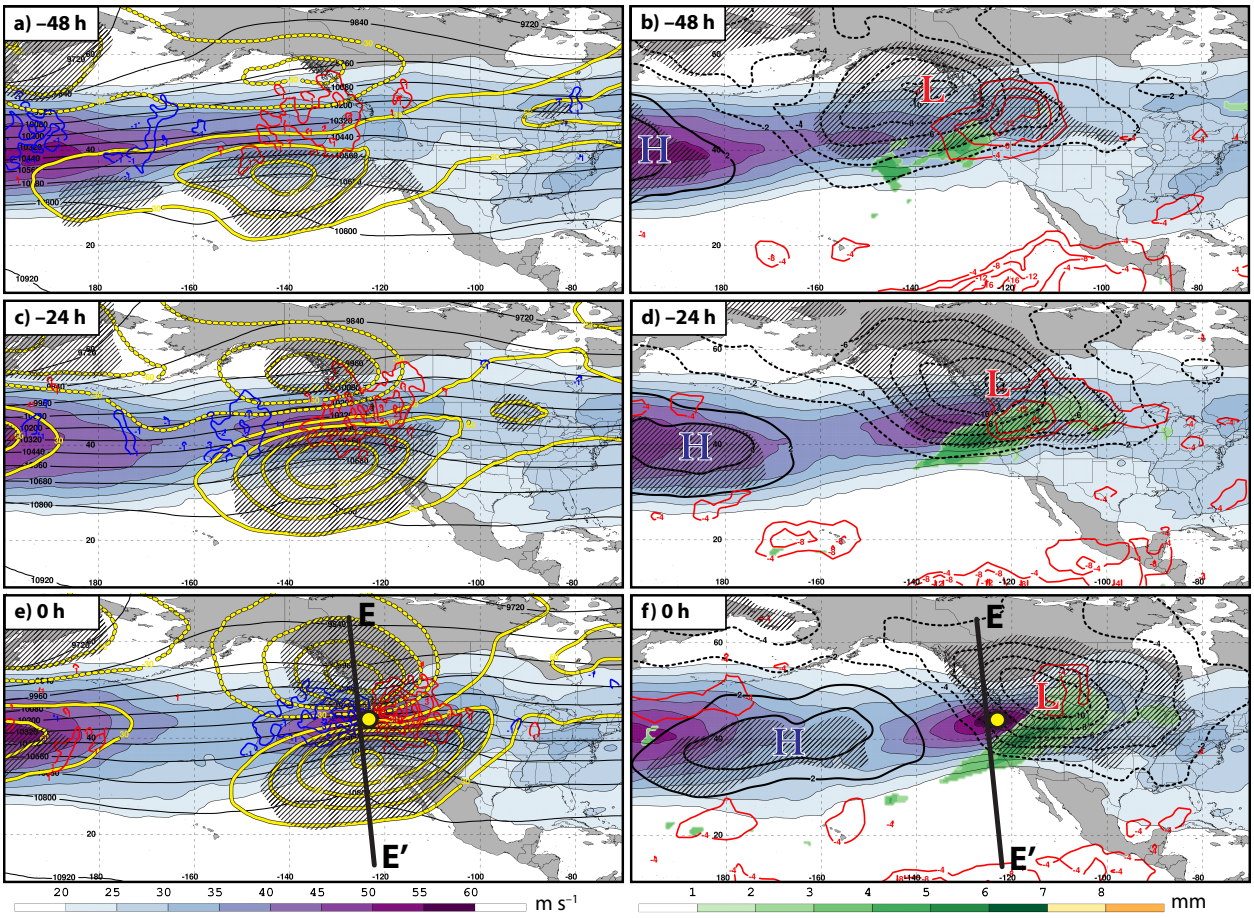

FIG. 10. Composite large-scale flow evolution prior to the initiation of a western subtropical dominant jet superposition event. All conventions are identical to those in Fig. 6.

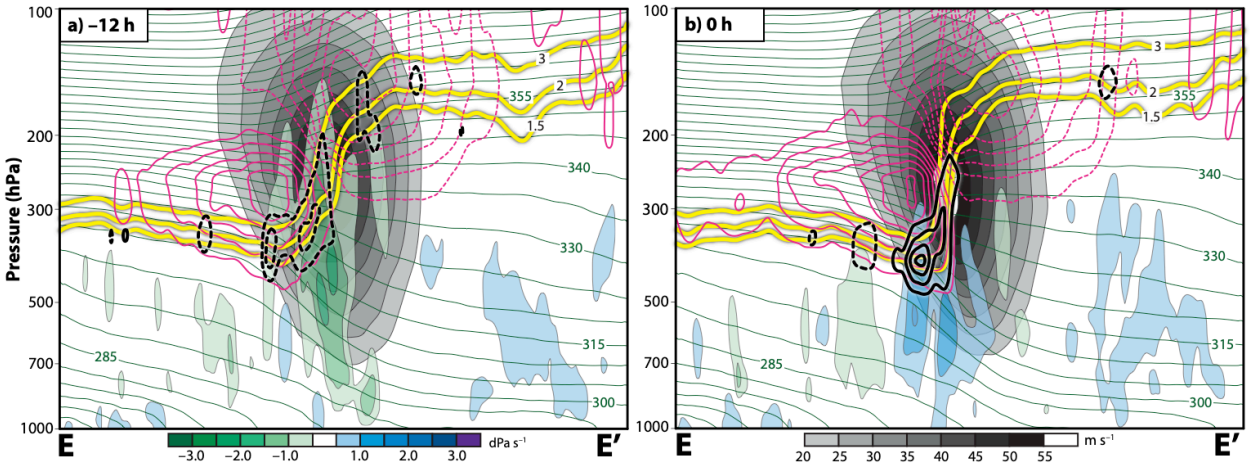

FIG. 11. (a) Cross section from E–E', as indicated in Figs. 10e,f, 12 h prior to a western subtropical dominant jet superposition event. All conventions are identical to those in Fig. 9. (b) As in (a), but for the cross section from E–E', as indicated in Figs. 10e,f, 0 h prior to a western subtropical dominant jet superposition event.

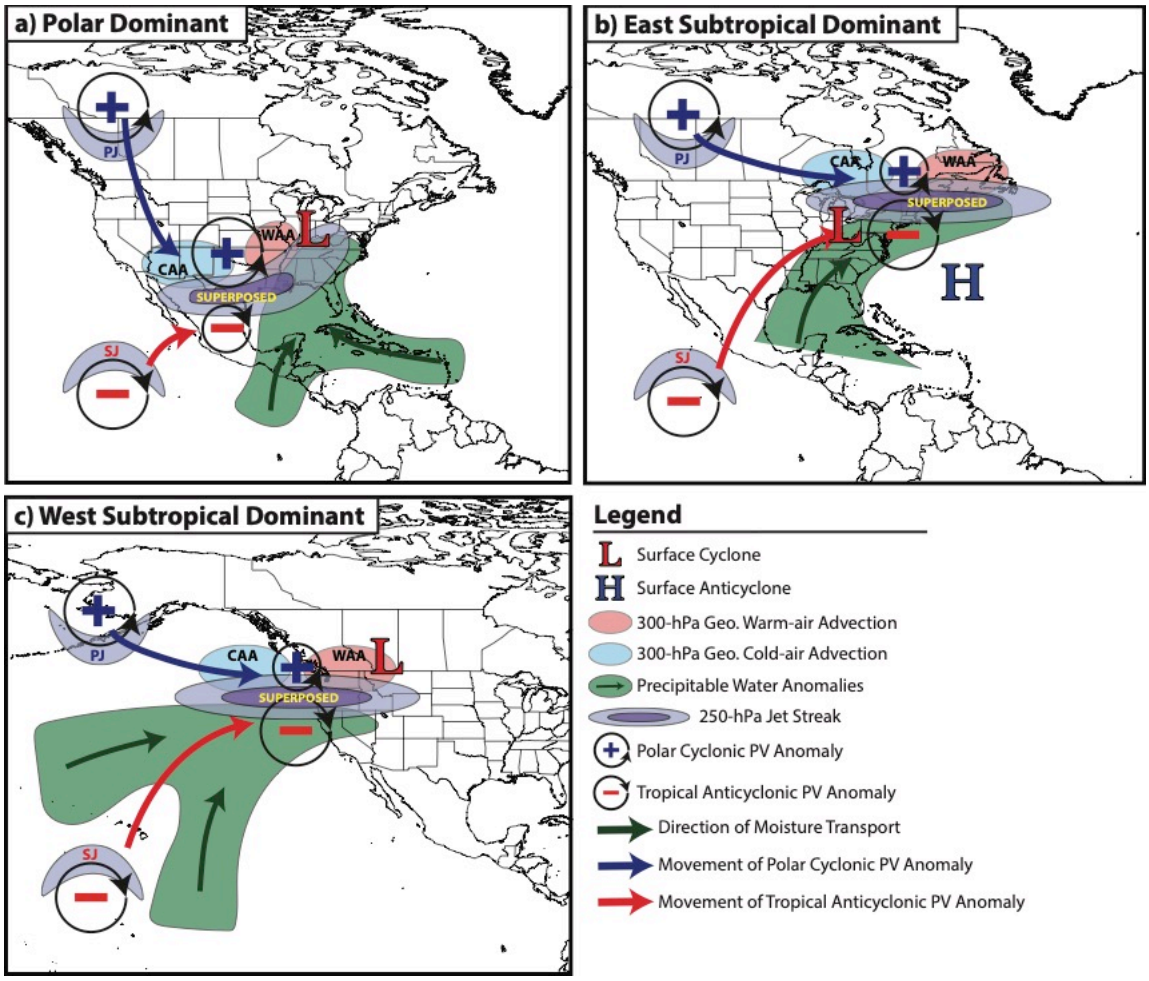

FIG. 12. Conceptual models for the development of (a) polar dominant, (b) eastern subtropical dominant, and (c) western subtropical dominant jet superposition events.